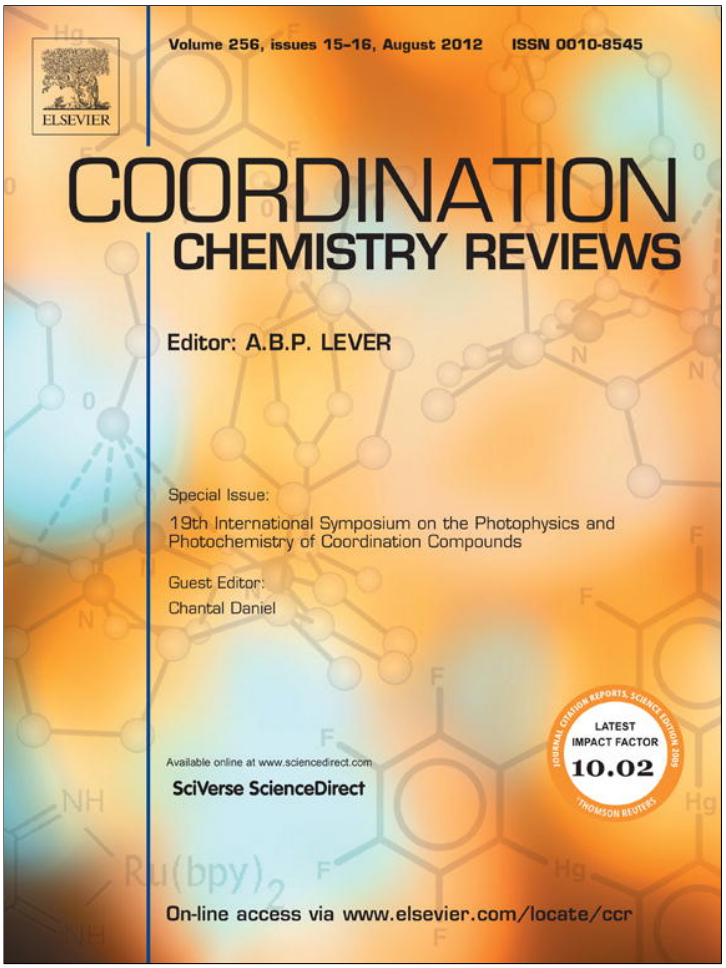

Coordination Chemistry Reviews 256 (2012) 1644–1663

Contents lists available at SciVerse ScienceDirect

Coordination Chemistry Reviews

journal homepage: www.elsevier.com/locate/ccr

Review

Optical sensitization and upconversion in discrete polynuclear chromium–lanthanide complexes

Lilit Aboshyan-Sorgho [a], Martine Cantuel [a], Stephane Petoud [c], Andreas Hauser [b], Claude Piguet [a,*]

[a] Department of Inorganic, Analytical and Applied Chemistry, University of Geneva, 30 quai E. Ansermet, CH-1211 Geneva 4, Switzerland
[b] Department of Physical Chemistry, University of Geneva, 30 quai E. Ansermet, CH-1211 Geneva 4, Switzerland
[c] Centre de Biophysique Moléculaire, CNRS UPR 4301, Rue Charles-Sadron, 45071 Orléans Cedex 2, France

Contents

ARTICLE INFO

Article history:
Received 27 October 2011
Received in revised form
19 December 2011
Accepted 19 December 2011
Available online 11 January 2012

Keywords:
Chromium(III)
Lanthanide(III)
Photophysics
Polynuclear complexes
Sensitization
Upconversion

ABSTRACT

Due to its extreme kinetic inertness, trivalent chromium, Cr(III), has been rarely combined with labile trivalent lanthanides, Ln(III), to give discrete self-assembled (supra)molecular polynuclear complexes. However, the plethora of accessible metal-centered excited states possessing variable lifetimes and emissive properties, combined with the design of efficient intramolecular Cr(III) ↔ Ln(III) energy transfer processes open attractive perspectives for programming directional light-conversion within these heterometallic molecules. Efforts made to address this exciting challenge for both light-sensitization and light-upconversion are discussed in this article.

1. Introduction and background

As independent cations, trivalent chromium, Cr(III), and trivalent lanthanides, Ln(III), display some striking optical similarities. Therefore, their combination within the same molecular architecture is expected, at first sight, to show some redundancy. However, there are also notable differences, which can be exploited to some advantage in mixed systems. Let's start with Ln(III) ions, which are well-known to possess numerous long-lived luminescent excited states leading to narrow emission bands with very small (if any) Stokes shifts. These optical characteristics result from (i) the atomic character of the shielded 4f valence electrons in chemical compounds and (ii) the parity selection rule which precludes intrashell 4f → 4f electric dipolar transitions [1]. Depending on its electronic configuration [Xe]$4f^n$ (n = 1–13), each open-shell trivalent lanthanide thus displays a specific distribution of excited states spanning from the ultraviolet (UV) to the near-infrared (NIR) regions of the electromagnetic spectrum, the exact energies of which can be tuned by crystal-field effects (Fig. 1) [2]. For trivalent chromium, the low-lying Cr(^{2}E) and Cr($^2T_1$) excited levels having the same $(t_{2g})^3$ electronic configuration as the Cr($^4A_2$) ground state in pseudo-octahedral complexes induce similar optical properties, i.e., long lifetimes, narrow emission bands with very small Stokes shifts and weak dependence on the chemical environment (Fig. 2) [3]. The alternative spin-allowed promotion of an electron from the Cr($^4A_2$) ground state into an anti-bonding orbital, resulting in a

* Corresponding author.
E-mail address: Claude.Piguet@unige.ch (C. Piguet).

0010-8545/$ – see front matter © 2011 Elsevier B.V. All rights reserved.
doi:10.1016/j.ccr.2011.12.013

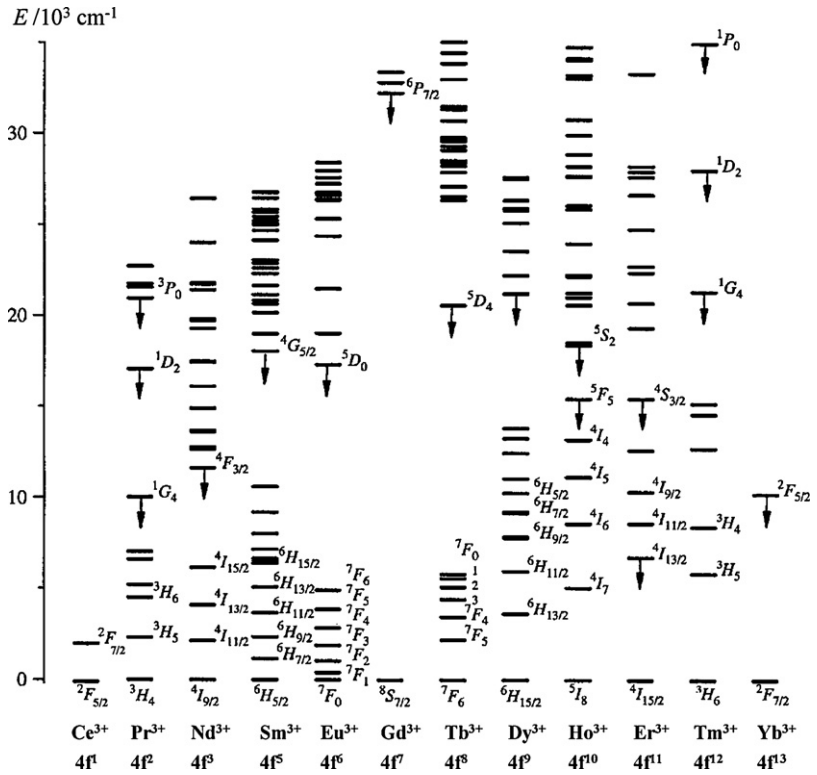

Fig. 1. Partial energy level diagram of non-radioactive open-shell Ln(III) ions according to Dieke. Downward arrows indicate standard emissive levels [2].

$(t_{2g})^2(e_g)^1$ electronic configuration, provides distorted Cr($^4T_2$) and Cr($^4T_1$) excited levels, whose energies are then highly sensitive to the ligand-field strength produced by the donor atoms coordinated to Cr(III) (Fig. 2a).

For donor atoms providing weak ligand-field strengths around Cr(III), such as those found in oxide or fluoride matrices, comparatively short-lived Cr($^4T_2 \rightarrow {}^4A_2$) fluorescence with a large Stokes shift or dual short-lived fluorescence and long-lived Cr(^2E, $^2T_1 \rightarrow {}^4A_2$) phosphorescence at low temperature are usually detected after irradiation (Fig. 2b) [4]. For strong-field ligands such as 2,2′-bipyridine [5] or cyanide [6] bound to Cr(III), the increased Cr($^4T_2$)-Cr(^2E) energy gap (Fig. 2a) speeds up the Cr($^4T_2 \rightarrow {}^2E$) intersystem crossing to such an extent that it becomes competitive with vibrational relaxation ($k_{ISC}^{Cr(^4T_2 \rightarrow {}^2E)} > 10^{13}\ s^{-1}$, $0.7 \leq \phi_{ISC}^{Cr(^4T_2 \rightarrow {}^2E)} \leq 1.0$). The lowest Cr($^2E$) excited state is thus efficiently fed and the characteristic deep red Cr(^2E, $^2T_1 \rightarrow {}^4A_2$) phosphorescence is the only emitted signal [3]. However, the phosphorescence quantum yields $\phi_P^{Cr(^2E \rightarrow {}^4A_2)}$ remain limited at room temperature for most strong-field Cr(III) complexes because of the effects of (i) thermally activated back intersystem crossing (BISC) [7] and/or (ii) surface crossing with a ground state intermediate [8].

Altogether, the low-lying Cr(^2E) excited state in strong-field pseudo-octahedral Cr(III) complexes is ideally suited (i) for operating as an efficient energy donor for sensitizing NIR-emissive lanthanides through intermetallic Cr → Ln energy transfer or (ii) for acting as the ultimate long-lived luminescent level following Ln → Cr energy transfer originating from UV or visible lanthanide emitters. It is worth to remind the reader here that the probability $W_{D,A}$ that a resonant energy transfer process occurs from a donor D to an acceptor A is given by Fermi's golden rule [9]

$$W_{D,A} = \frac{2\pi}{\hbar} \left| \langle DA^* | H | D^*A \rangle \right|^2 \Omega_{D,A} \quad (1)$$

H is the interaction Hamiltonian that mediates energy transfer from the excited donor D* to the ground state acceptor A. The interaction mechanism may be multipolar electrostatic or magnetic [10], or can be an exchange coupling [11]. $\Omega_{D,A}$ is the spectral overlap integral (Eq. (2)) where $g_D(E)$ and $g_A(E)$ are the normalized line shape functions for the homogeneous lines of the donor and acceptor, respectively.

$$\Omega_{D,A} = \int g_A(E) \cdot g_D(E)\, dE \quad (2)$$

$\Omega_{D,A}$ ensures energy conservation, and it is thus not too surprising that the low-lying Cr(^2E) level has been primarily exploited in co-doped solids and in coordination networks as donor level for resonant energy transfer toward Tm(III) [4], Nd(III) and Yb(III) [6], which possess compatible low-lying accepting levels (Fig. 3a). The alternative use of the Cr(^2E) excited level as acceptor level for collecting energy from high-energy Eu(III) and Tb(III) donors is much less frequent due to the large Eu($^5D_0$)-Cr(^2E) and Tb($^5D_4$)-Cr(^2E) energy gaps which minimize Ω_{DA}, a drawback partially overcomes by the presence of the Cr($^4T_1$, $^4T_2$) levels as relays in the global energy transfer mechanism (Fig. 3b) [12]. Moreover, the apparent invariance of the energy of the Cr(^2E) excited level in the Tanabe-Sugano diagram for almost any changes in chemical environment (Fig. 2a) may mislead non-specialists since both abscissa and ordinate of these diagrams are scaled by the interelectronic repulsion integrals expressed with the Racah parameter B. In octahedral symmetry, the energy of the spin-forbidden transition Cr($^2E \leftrightarrow {}^4A_2$) is given in Eq. (3), where B and C are the Racah parameters and Δ is the ligand-field splitting [13].

$$\Delta E = E\left[Cr\left(^2E\right)\right] - E\left[Cr\left(^4A_2\right)\right] = \frac{9B + 3C - 90B^2}{\Delta} \quad (3)$$

With the standard approximation that $C \approx 4B$ for coordination complexes with O-donor or N-donor atoms [14a], Eq. (3) reduces to Eq. (4).

$$\Delta E = E\left[Cr\left(^2E\right)\right] - E\left[Cr\left(^4A_2\right)\right] = \frac{21B - 90B^2}{\Delta} \quad (4)$$

Table 1
Ligand-field parameters (Δ), interelectronic repulsion parameters (B), energies of the $Cr(^2E)$ level and $E(Cr(^4T_2))$-$E(Cr(^2E))$ energy gaps in selected pseudo-octahedral Cr(III) complexes [13,14].[a]

Complex	Δ/cm^{-1}	B/cm^{-1}	Δ/B	$E(Cr(^2E))$/cm^{-1}	$E(Cr(^4T_2))$-$E(Cr(^2E))$[b]/cm^{-1}
Cr^{3+}	0	918	0	16,065	
$[Cr(OH_2)_6]^{3+}$	18,000	870	20.7	15,000	1500
$[Cr(NH_3)_6]^{3+}$	21,640	878	24.6	15,230	5000
$[Cr(bipy)_3]^{3+}$	23,240	761	30.5	13,740	8000
$[Cr(CN)_6]^{3-}$	26,400	660	40.0	12,370	12,500

[a] The approximation $C = 4B$ is used for the coordination complexes except for $[Cr(OH_2)_6]^{3+}$ in which $C = 4.2B$ is applied [14a].
[b] $E(Cr(^4T_2))$-$E(Cr(^2E))$ is estimated from the Franck-Condon energies of the respective transitions from the ground state and corrected for the reorganization energy of the $^4T_2$ state of typically 1500 cm^{-1}.

The small second-order dependence of ΔE on Δ is offset by the reduction of B and C due to the nephelauxetic effect resulting in an overall red-shift of the $Cr(^4A_2 \rightarrow {}^2E)$ transition with increasing ligand-field strength. This can be verified with an inspection of standard pseudo-octahedral Cr(III) complexes showing that the $Cr(^2E)$-$Cr(^4A_2)$ energy gaps indeed span the 12,000–15,000 cm^{-1} range along the nephelauxetic series $B(OH_2) \approx B(NH_3) > B(bipy) > B(CN)$ (Table 1, [13,14]), a phenomenon which is at the origin of the optimization of the energy of the $Cr(^2E)$ level for maximizing the spectral overlap in intermetallic energy transfer [6,12]. Δ corresponds directly to the maximum of the $Cr(^4A_2 \rightarrow {}^4T_2)$ absorption band [14], and thus the variation of the $Cr(^4T_2)$-$Cr(^2E)$ energy gap depends strongly on Δ. In fact, the latter can be estimated from the difference in energy of the corresponding optical transitions corrected for the total reorganization energy of the $^4T_2$ state of typically 1500 cm^{-1}.

Returning to the Tanabe-Sugano diagram, the $\Delta/B \approx 20.7$ ratio found for $[Cr(OH_2)_6]^{3+}$ corresponds to $E(Cr(^2E)) \approx E(Cr(^4T_2))$ (Fig. 4),

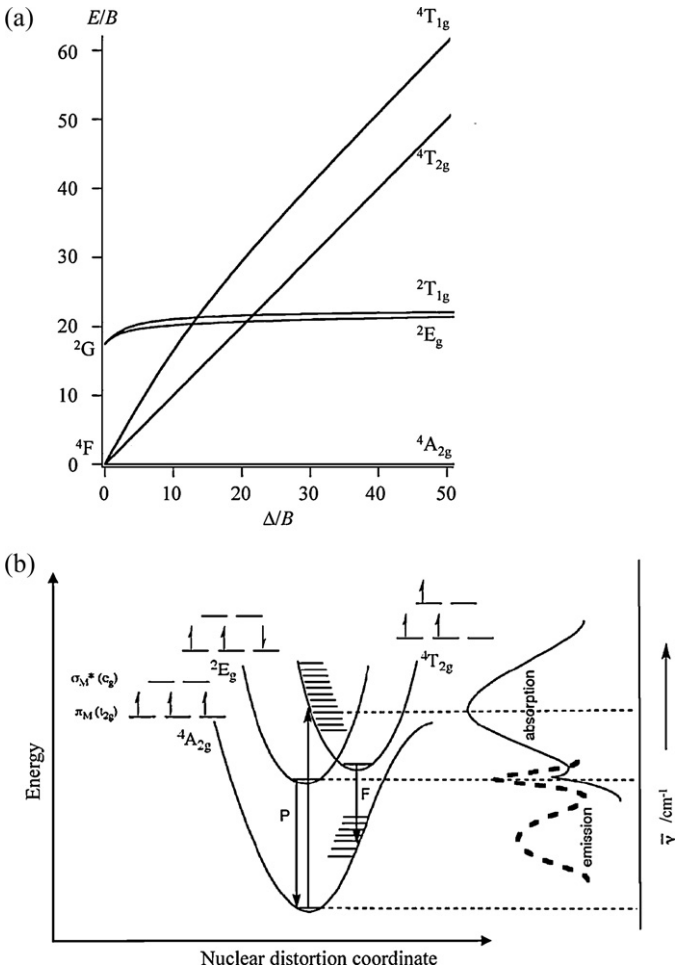

Fig. 2. a) Simplified Tanabe-Sugano type diagram for the d^3 electronic configuration in O_h symmetry and b) schematic potential surface diagram for an octahedral Cr(III) complex depicting its relationship with electronic configurations and with absorption and emission spectra (F = fluorescence, P = phosphorescence).
Adapted from [3b].

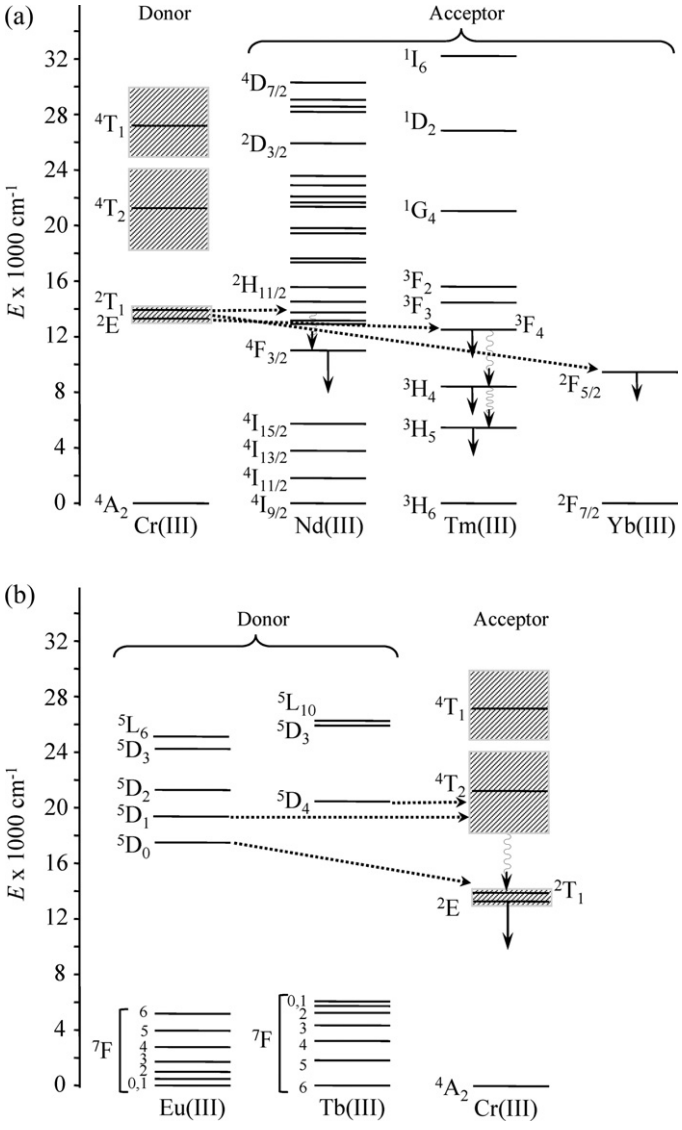

Fig. 3. Partial energy level diagrams representing the electronic structure of a strong-field Cr(III) complex acting as a) a donor [4,6] and b) an acceptor [12] in Cr ↔ Ln energy transfer processes occurring in doped solids or coordination networks. Horizontal dotted arrows = resonant energy transfer, bent dotted arrows = phonon-assisted energy transfer, straight down full arrows = emissive levels and undulating downward arrows = internal conversion.

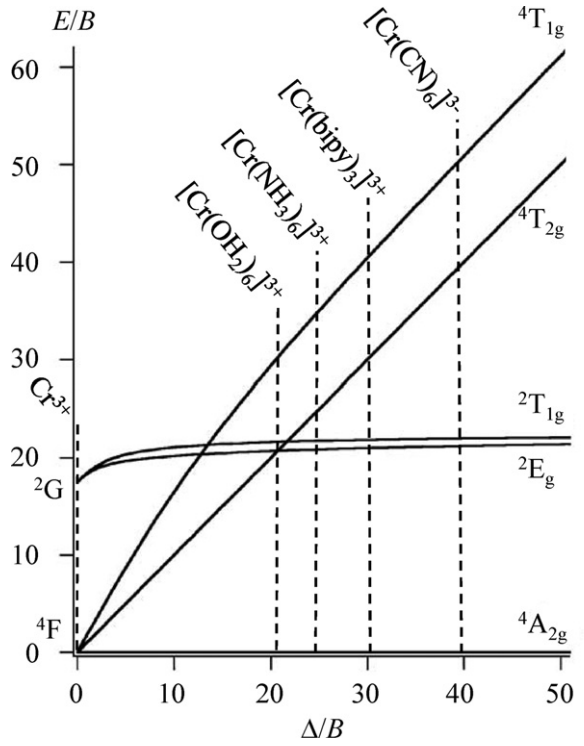

Fig. 4. Simplified Tanabe-Sugano type diagram for the d^3 electronic configuration in O_h symmetry showing the location of Cr^{3+}, $[Cr(OH_2)_6]^{3+}$, $[Cr(NH_3)_6]^{3+}$, $[Cr(bipy)_3]^{3+}$ and $[Cr(CN)_6]^{3-}$.

and dual short-lived $Cr(^4T_2 \rightarrow {}^4A_2)$ fluorescence and long-lived $Cr(^2E \rightarrow {}^4A_2)$ phosphorescence thus result, together with efficient thermally activated quenching of the $Cr(^2E)$ excited state by back intersystem crossing. This unfavorable situation is typical for CrO_6 chromophores, and it did not strongly encourage the use of Cr(III) as a donor for NIR lanthanide emitters in co-doped solid-state oxide matrices [4,5].

We however note that Güdel and coworkers demonstrated that YAG and YGG matrices (YAG = YAl_5O_{12}, YGG = YGa_5O_{12}) co-doped with Cr(III) and Yb(III) exhibit $Cr(^2E)Yb(^2F_{7/2}) \rightarrow Cr(^4A_2)Yb(^2F_{5/2})$ energy transfer leading to an efficient low temperature (13 K) optical light-downconversion from laser excitation of the $Cr(^2E, {}^4T_2 \leftarrow {}^4A_2)$ transition in the 21,000–15,000 cm^{-1} domain into the NIR domain of the $Yb(^2F_{5/2} \rightarrow {}^2F_{7/2})$ transition at 10,400 cm^{-1} [15]. The reverse optical process, i.e. NIR to visible upconversion, benefits from the low-phonon energy of these solid matrices and selective irradiation of the $Yb(^2F_{7/2} \rightarrow {}^2F_{5/2})$ transition at 10,315 cm^{-1} is followed by a cooperative sensitization mechanism which excites Cr(III) to its $Cr(^4T_1)$ state (Fig. 5). Subsequent internal conversion and intersystem crossing eventually feed the $Cr(^2E)$ state, which emits in the red [15]. Repeating these experiments with $YAlO_3$ as the host matrix gave similar results except for the involvement of [Cr(III)Cr(III)] pairs as the emissive species [16].

For *N*-donor ligands in $[Cr(NH_3)_6]^{3+}$, $[Cr(bipy)_3]^{3+}$ or C-donor ligands in $[Cr(CN)_6]^{3-}$, larger Δ/B ratios correspond to larger $Cr(^4T_2)$-$Cr(^2E)$ energy gaps (Table 1, column 6 and Fig. 4) which limit unfavorable back intersystem crossing processes and thus favor efficient intermetallic $Cr(^2E) \rightarrow Ln(III)$ energy transfer. However, easy-handled solid-state host matrices providing octahedral N_6 or C_6 environments are essentially unknown. Therefore, the targeted strong-field $[CrN_6]$ and $[CrC_6]$ chromophores should be designed by coordination chemistry, but the extreme kinetic inertness of the half-filled shell $(t_{2g})^3$ electronic configuration found in octahedral Cr(III) complexes, usually prevents exploitable

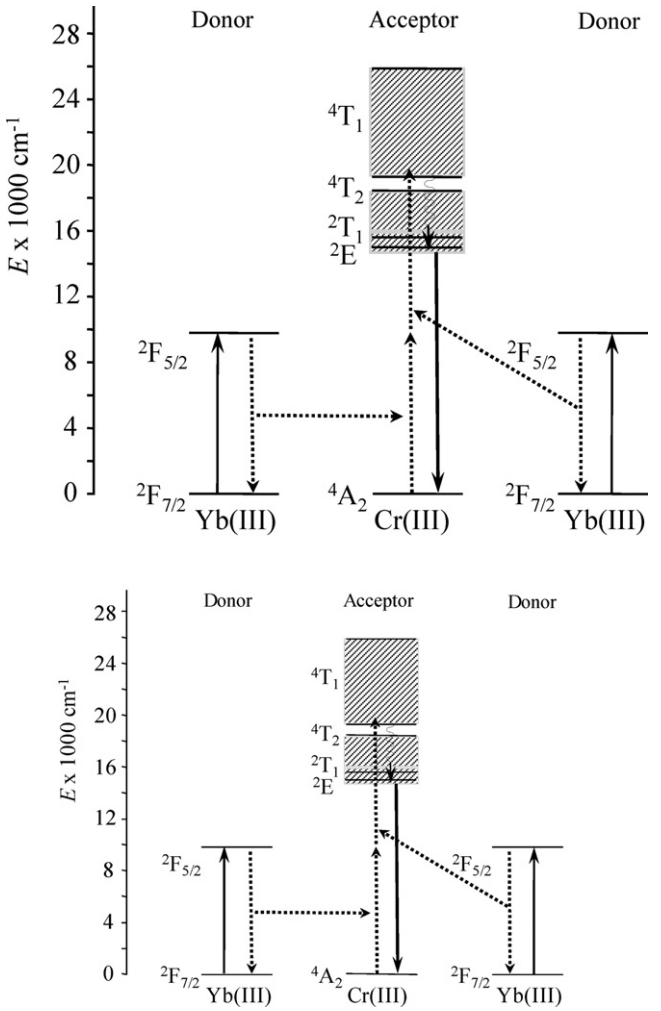

Fig. 5. Schematic diagram representing the cooperative sensitization of Cr(III) luminescence by two excited Yb(III) ions in YAG matrices. Straight upward arrows = excitation, dotted arrows = non-radiative energy transfer, undulating arrow = non-radiative multiphonon relaxation and straight downward arrow = luminescence step.
Adapted from refs. [15] and [16].

ligand-exchange under standard conditions [17]. The introduction of Cr(III)/Ln(III) pairs within the same chemical architecture thus relies either on high temperature melting processes (as found for co-doped oxide matrices), or on ionic associations of inert pre-formed pseudo-octahedral Cr(III) precursors, for instance $[Cr(oxalate)_3]^{3-}$ [18], $[Cr(CN)_6]^{3-}$ [6], $[Cr(bipy)(oxalate)_2]^-$ [19], $[Cr(urea)_6]^{3+}$, $[Cr(ethylenediamine)_3]^{3+}$ or $[Cr(sarcophagine)]^{3+}$ [12], with solvated Ln^{3+} counter-cation or $[Ln(2,6\text{-dipicolinate})_3]^{3-}$ counter-anions. Efficient $Tb \rightarrow Cr$ and $Eu \rightarrow Cr$ energy transfers were characterized in the solid state with $[CrN_6]$ chromophores acting as acceptors [12], whereas the strong-field $[CrC_6]$ chromophore in $[Cr(CN)_6]^{3-}$ was shown to be a remarkable donor for sensitizing Yb(III) and Nd(III) NIR emitters [6]. The destruction of these networks in solution removes permanent Cr–Ln interactions and bans the use of these systems as engineered time-gated luminescent probes for analytical, biological and medical applications. This review therefore aims at encouraging coordination chemists to explore this as yet unexplored field, and it therefore focuses on the synthesis and characterization of the rare examples of discrete (supra)molecular Cr–Ln systems whose structural integrity and optical properties are maintained in solution and/or in the gas-phase. Some partial reports of the photophysical properties of

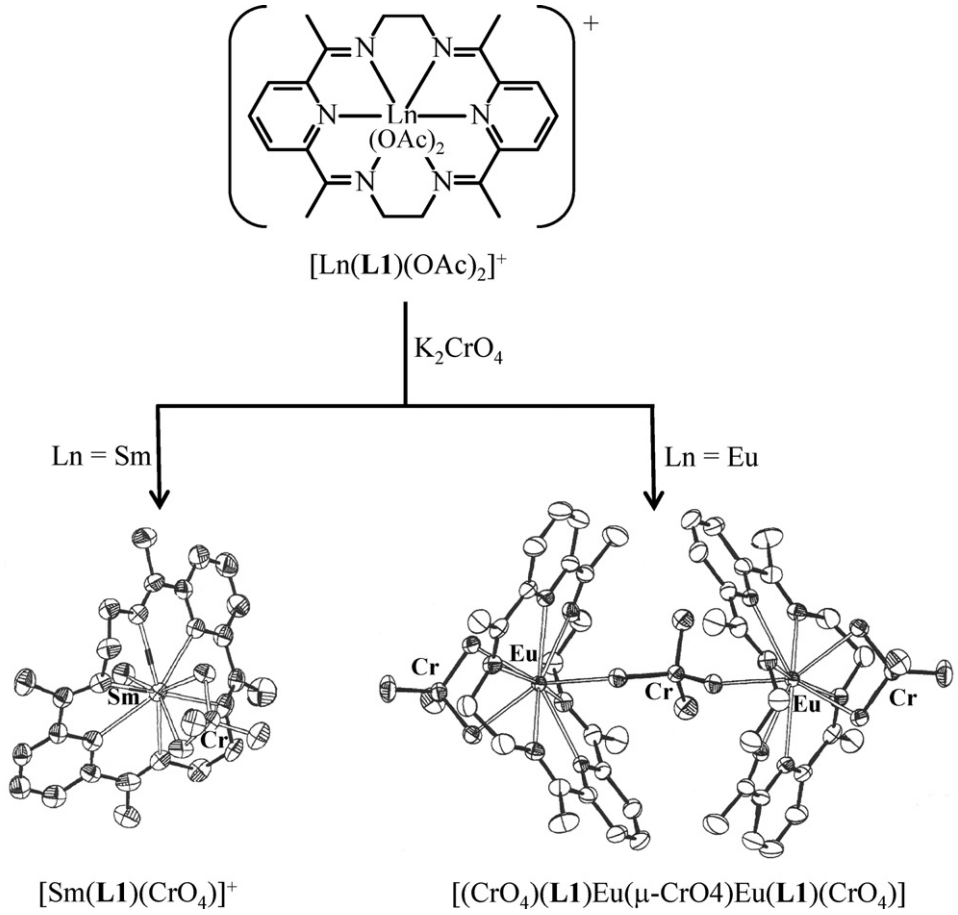

Fig. 6. Synthesis and structures of chromate–Ln(III) complexes [22].

discrete Cr(III)/Ln(III) pairs can be found in two extended reviews dedicated to the sensitization of trivalent lanthanides in d–f heteronuclear arrays [20].

2. Synthetic strategies for the preparation of discrete polynuclear Cr–Ln complexes

Due to the distribution of the three valence electrons into the t_{2g} orbitals directed between the metal–ligand bonds in octahedral Cr(III) complexes, associative ligand-exchange pathways involving putative high-energy seven-coordinate intermediates are expected to be very slow [17,21]. The alternative dissociative mechanisms through five-coordinate intermediates suffer from the large ligand-field stabilization energy found for d^3 system in octahedral symmetry [21]. Cr(III) complexes are thus famous in coordination chemistry for their exceptional kinetic inertness and for their exclusive stereochemical preference for octahedral geometry. Three strategies have been developed for overcoming this limitation with the ultimate goal of incorporating Cr(III)/Ln(III) pairs into discrete coordination complexes.

(1) Firstly, highly oxidizing Cr(VI) species (usually chromate $[CrO_4]^{2-}$ or dichromate $[Cr_2O_7]^{2-}$) are reduced in presence of stable Ln(III) complexes in order to produce heteronuclear Cr–Ln architectures. To the best of our knowledge, the precursor chromate complexes $[Sm(\mathbf{L1})(CrO_4)(H_2O)]^+$ and $[(CrO_4)(\mathbf{L1})Eu(\mu\text{-}CrO_4)Eu(\mathbf{L1})(CrO_4)]$ are rare examples of this synthetic strategy, but no reduced Cr(III)/Ln(III) complexes could be characterized (Fig. 6) [22]. On the contrary, high temperature air oxidation of $[Cr^{III}(urea)_6][Ln(dipicolinate)_3]$ resulted in mixtures of chromate $LnCrO_4$ and chromite $LnCrO_3$ (perovskite) [23].

(2) The second method overcomes the kinetic activation barrier for ligand-exchange in Cr(III) complexes by vigorous thermal heating like the one used for the doping of solid-state matrices with Cr(III)/Ln(III) pairs. This approach was successful for the synthesis of inert mononuclear $[Cr(ox)_3]^{3-}$ (ox = oxalate) [24], $[(acac)_2Cr(ox)]^-$ (acac = acetylacetonate) [25] and $[(acac)_2Cr(bpypz)]$ (bpypz = 3,5-bis(2-pyridyl)pyrazolate) [26] complexes, which were further reacted with protected Ln(III) complexes $\{[Cu(\mathbf{L})(H_2O)]_2Ln(H_2O)_2\}$, $[Ln(HB(pz)_3)_2]^+$ ($HB(pz)_3$ = trispyrazolyl borate) or $[Ln(hfac)_3]$ (hfac = hexafluoroacetylacetonate) to give the ternary complexes $\{(ox)_2Cr(ox)Ln(H_2O)_2[Cu(\mathbf{L})(H_2O)]_2\}$, $[(acac)_2Cr(ox)Ln(HB(pz)_3)_2]^-$ and $[(acac)_2Cr(bpypz)Ln(hfac)_3]$ (Fig. 7). More sophisticated inert Cr(III)-containing polyoxometallate precursors $\{(\gamma\text{-}SiW_{10}O_{36})_2[Cr(OH)(H_2O)_3]_3\}^{10-}$ [27] and $[Cr(OH)_6Mo_6O_{18}]^{3-}$ [28] have also been prepared, but their reactions with Ln(III) only resulted in coordination polymers. Whereas electrochemistry and electronic spectroscopies (absorption, circular dichroïsm (CD) and magnetic circular dichroïsm (MCD)) confirmed the formation of discrete dinuclear dimetallic complexes in solution for $[(acac)_2Cr(ox)Ln(HB(pz)_3)_2]^-$ and $[(acac)_2Cr(bpypz)Ln(hfac)_3]$ [25,26], the tetranuclear trimetallic complexes $\{(ox)_2Cr(ox)Ln(H_2O)_2[Cu(\mathbf{L})(H_2O)]_2\}$ were only characterized in the solid state [24]. The only justification for their classification as discrete molecular entities resulted from the weak hydrogen bonding network

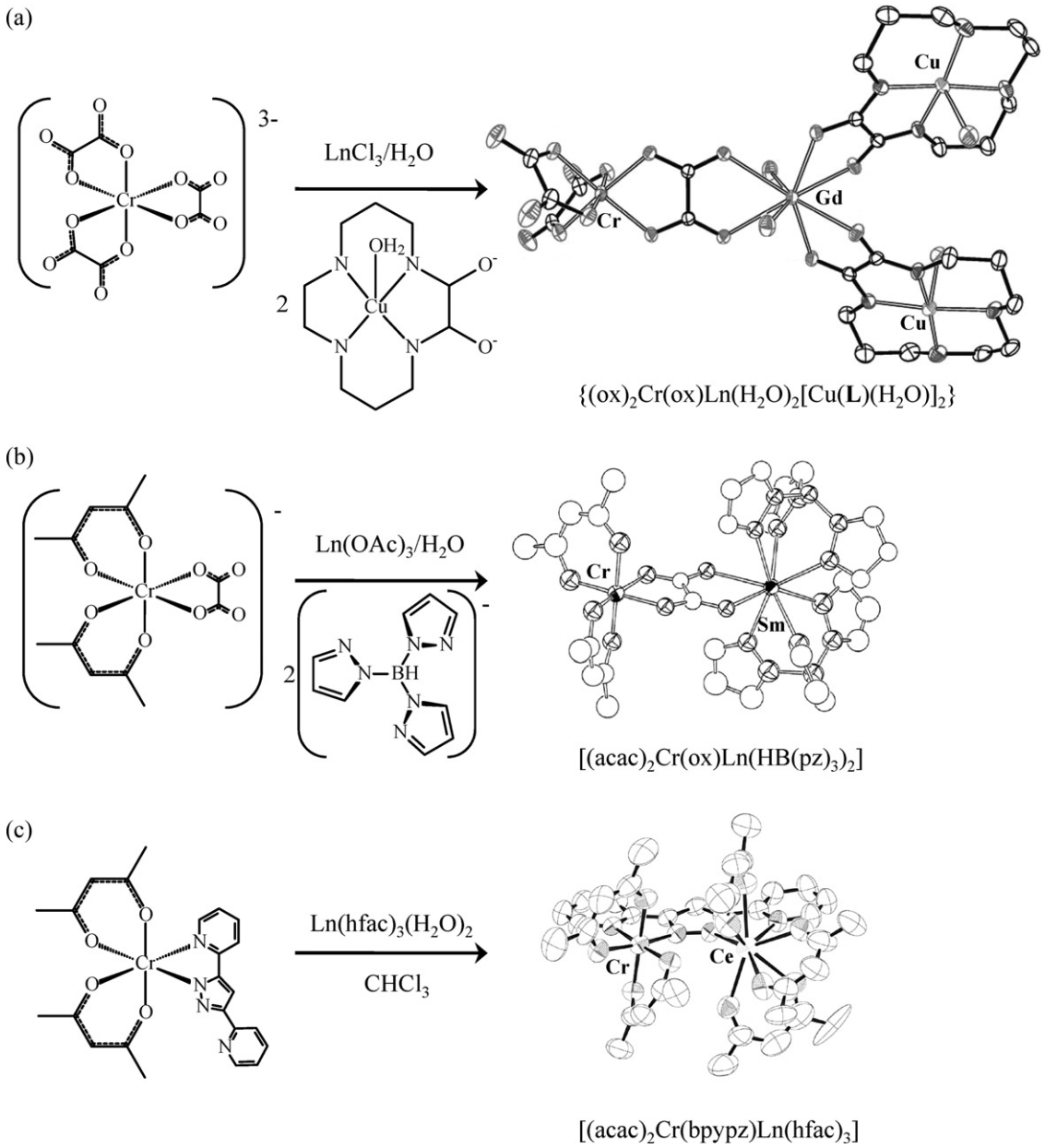

Fig. 7. Synthesis and structures of a) $\{(ox)_2Cr(ox)Ln(H_2O)_2[Cu(\mathbf{L})(H_2O)]_2\}$ [24], b) $[(acac)_2Cr(ox)Ln(HB(pz)_3)_2]^-$ [25] and c) $[(acac)_2Cr(bpypz)Ln(hfac)_3]$ [26].

responsible for the intermolecular cohesion between $\{(ox)_2Cr(ox)Ln(H_2O)_2[Cu(\mathbf{L})(H_2O)]_2\}$ units in the crystalline state.

(3) Finally, the third strategy relies on thermodynamic self-assembly, which proved to be so efficient for preparing sophisticated polynuclear lanthanide-containing aggregates [29]. Unfortunately, it fails with Cr(III)/Ln(III) pairs because of the kinetic inertness of Cr(III), which precludes the complete exploration of the energy hypersurface [30] as previously reported for Ru(II)/Ln(III) [31] and Os(II)/Ln(III) pairs [32]. For the related inert low-spin d^6 octahedral Co(III) cation, this limitation was overcome with the introduction of Co(II)/Ln(III) precursor pairs, which led to the quantitative self-assembly of $[LnCo^{II}(\mathbf{L2})_3]^{5+}$ as triple-stranded helicates in solution. Subsequent bromine oxidation quantitatively yielded inert $[LnCo^{III}(\mathbf{L2})_3]^{6+}$ complexes [33]. Considering that the lability of ligand-exchange processes around chromium cations increases by 14 orders of magnitude on going from $[Cr^{III}(H_2O)_6]^{3+}$ ($k_{exch(298\,K)} = 2.4 \times 10^{-6}\ s^{-1}$, [17b]) to $[Cr^{II}(CH_3OH)_6]^{2+}$ ($k_{exch(298\,K)} = 1.2 \times 10^{8}\ s^{-1}$, [34]), Cr(II)/Ln(III) pairs are thus good candidates for thermodynamic self-assembly, whereas oxidative post-modification should lead to the targeted inert Cr(III)/Ln(III) complexes. Taking advantage of the limited dependence of the electrochemical Cr(III)/Cr(II) reduction potential on ligand variation ($E^\circ([Cr(NH_3)_6]^{3+}/[Cr(NH_3)_6]^{2+}) = -0.63$ V $E^\circ([Cr(H_2O)_6]^{3+}/[Cr(H_2O)_6]^{2+}) = -0.41$ V and $E^\circ([Cr(bipy)_3]^{3+}/[Cr(bipy)_3]^{2+}) = -0.25$ V vs. NHE [13,35]), a large number of Cr(III) complexes may be thus easily prepared by simple air oxidation of their Cr(II) precursors. This strategy, originally used for the preparation of mononuclear $[Cr(bipy)_3]^{3+}$ complexes [5b], was extended for the synthesis of dinuclear $[CrLn(\mathbf{L2})_3]^{6+}$ [36] and trinuclear $[CrLnCr(\mathbf{L3})_3]^{9+}$ helicates (Fig. 8) [37].

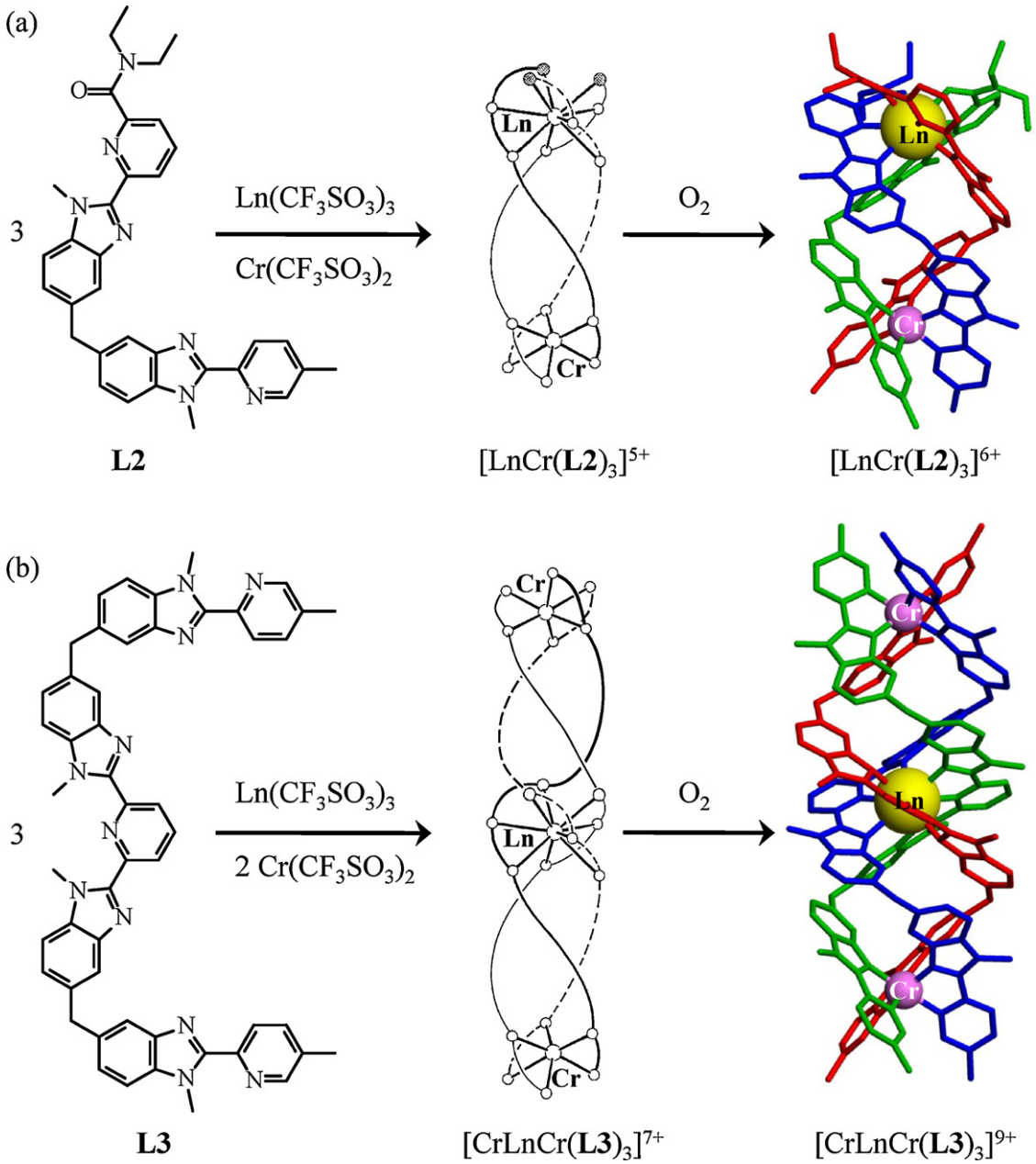

Fig. 8. Thermodynamic self-assembly with post-modification of a) dinuclear $[CrLn(\mathbf{L2})_3]^{6+}$ [36] and b) trinuclear $[CrLnCr(\mathbf{L3})_3]^{9+}$ triple-stranded helicates [37].

3. Characterization of discrete polynuclear Cr–Ln complexes

Although the heterometallic Cr–Ln complexes shown in Figs. 7 and 8 are considered as discrete molecular entities, their structural characterizations essentially rely on solid-state X-ray diffraction data. As expected, the Cr(III) cations systematically adopt pseudo-octahedral coordination geometries fitted with either O-donor or N-donor atoms, while the chemical environments around Ln(III) change from pseudo-square antiprismatic eight-coordination in $\{[(ox)_2Cr(ox)Ln(H_2O)_2[Cu(\mathbf{L})(H_2O)]_2\}$, $[(acac)_2Cr(ox)Ln(HB(pz)_3)_2]^-$ and $[(acac)_2Cr(bpypz)Ln(hfac)_3]$ (Fig. 7) to pseudo-tricapped trigonal prismatic nine-coordination in $[CrLn(\mathbf{L2})_3]^{6+}$ and $[CrLnCr(\mathbf{L3})_3]^{9+}$ (Fig. 8). The intramolecular intermetallic Cr···Ln contact distances (5.82 Å in $\{[(ox)_2Cr(ox)Gd(H_2O)_2[Cu(\mathbf{L})(H_2O)]_2\}$, 5.63 Å in $[(acac)_2Cr(ox)Yb(HB(pz)_3)_2]$, 4.58 Å in $[(acac)_2Cr(bpypz)Gd(hfac)_3]$, 9.33 Å in $[CrYb(\mathbf{L2})_3]^{6+}$ and 8.59–8.91 Å in $[CrEuCr(\mathbf{L3})_3]^{9+}$) are 20–50% shorter than the closest intermolecular Cr···Cr, Cr···Ln or Ln···Ln interactions in the crystalline state. This latter observation can be considered as a strong indication of the 'molecular behavior' of these dinuclear and trinuclear complexes [24–26,36,37]. However, no additional proof is at hand for the existence of isolated $\{[(ox)_2Cr(ox)Gd(H_2O)_2[Cu(\mathbf{L})(H_2O)]_2\}$ or $[(acac)_2Cr(bpypz)Gd(hfac)_3]$ entities in solution and their discrete character remains debatable. The latter two compounds will be therefore no more considered for the remainder of this review. Fast Atom Bombardment Mass Spectrometric (FAB-MS) data collected for $[(acac)_2Cr(ox)Ln(HB(pz)_3)_2]$ in a liquid nujoll matrix are the only direct proof for the existence of isolated discrete entities [25a], but the electronic spectra (absorption, NIR-CD, CD, MCD and emission) recorded in dichloromethane provide convincing support for (i) the assignment of the local chemical environment of the metal ions (pseudo-octahedral for

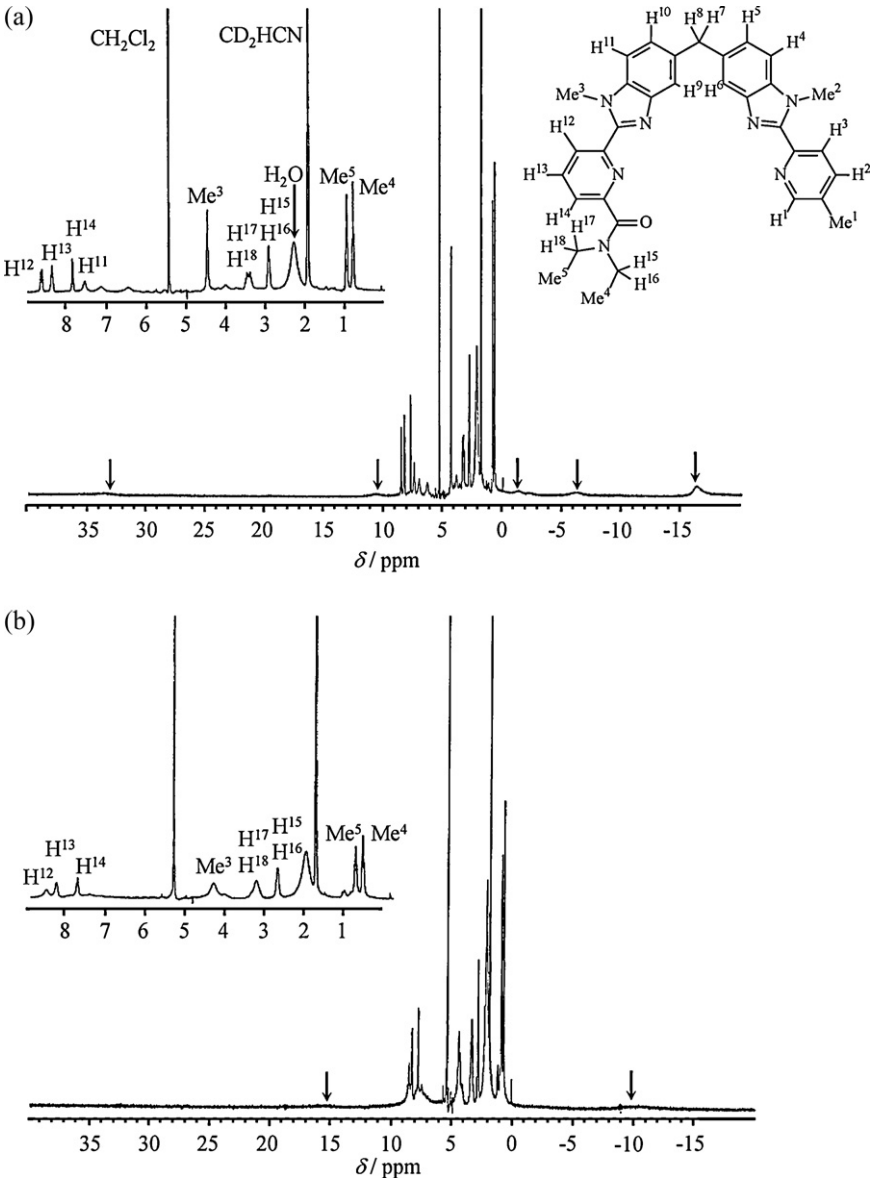

Fig. 9. ^{1}H NMR spectra of a) HHH-[LaCr^{II}(**L2**)$_3$]$^{5+}$ and b) HHH-[LaCr^{III}(**L2**)$_3$]$^{6+}$ in CD_3CN with numbering scheme and partial assignment (HHH stands for head-to-head-to-head, arrows indicate broadened paramagnetic signals).
Adapted from [36a].

Cr(III) and pseudo-square antiprismatic for Ln(III)) and (ii) the trigonal arrangement of three aromatic chromophores around Cr(III) [24]. The lack of concentration-dependent analyses of these spectroscopic data collected in solution precludes any reliable estimation of putative partial dissociation of the capping $[Ln(HB(pz)_3)_2]^+$ units, a phenomenon which may significantly affect the interpretation of electronic spectra at low concentrations. Such difficulties are inherent to open-shell Cr(III) complexes because of the slow characteristic electronic relaxation time ($\tau_e \approx 10^{-9}$ s at room temperature) associated with the orbitally non-degenerate paramagnetic $Cr^{III}(^4A_2)$ ground state, which prevents the recording of high-resolution NMR spectra (Fig. 9b) [38]. Interestingly, this limitation may be partially overcome for low-spin Cr(II) precursors since the paramagnetic $Cr^{II}(^3T_1)$ ground state possesses fast electronic relaxation ($\tau_e \approx 10^{-12}$ s) [39] and minor electronic delocalization [40]. The reversible redox Cr(III)/Cr(II) process thus offers an under-exploited strategy for the complete characterization of discrete Cr–Ln aggregates in solution (Fig. 9). Combined with the exclusive detection of $[CrLn(\mathbf{L2})_3]^{6+}$ and $[CrLnCr(\mathbf{L3})_3]^{9+}$ (and their gas-phase adducts formed with triflate counter-anions) by ElectroSpray Ionization Mass Spectrometry (ESI-MS, Fig. 10), the NMR spectroscopic data collected for Cr(II) and Cr(III) complexes are reliable proofs for the existence of these charged species as discrete Cr–Ln complexes in solution [36,37].

Partial decomplexation of the Ln(III) part may be problematic in solution when isolated Cr–Ln pairs are the subject of spectroscopic investigations. For instance, millimolar acetonitrile solutions of the C_3-symmetrical dinuclear helicates HHH-$[LnCr(\mathbf{L2})_3]^{6+}$ quantitatively produce HHH-$[Cr(\mathbf{L2})_3]^{3+}$ (HHH stands for head-to-head-to-head) and solvated Ln^{3+} upon treatment with water (14 M), or HHH-$[Cr(\mathbf{L2})_3]^{3+}$ and $[Ln(EDTA)]^-$ upon reaction with (nBu_4N)EDTA (1 eq.). A thorough thermodynamic study indicates that the formation constants $\log(\beta_{1,1}^{[Cr(\mathbf{L2})_3],Ln}) = 5.3–5.9$ estimated for Eq. (5) are responsible for 10–50% of lanthanide decomplexation

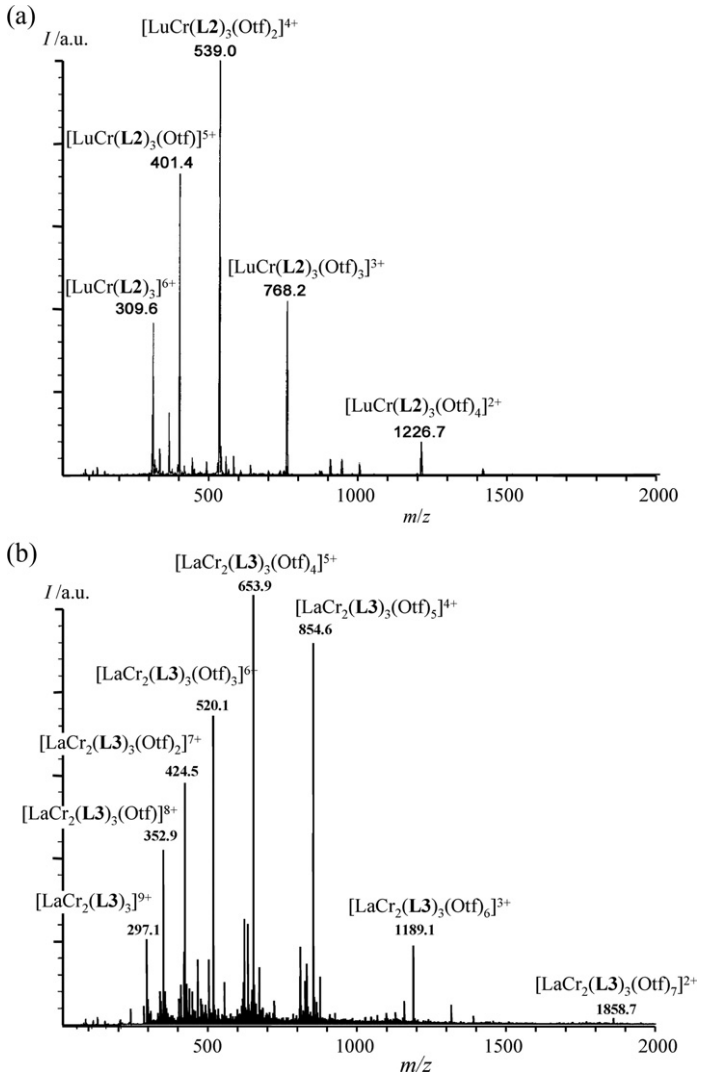

Fig. 10. ESI-MS spectra of a) HHH-[LuCr(**L2**)$_3$]$^{6+}$ and b) [CrLaCr(**L3**)$_3$]$^{9+}$ in CH_3CN (HHH stands for head-to-head-to-head). Adapted from [36a] and [37b].

in 10^{-5} M acetonitrile solutions of HHH-[LnCr(**L2**)$_3$]$^{6+}$, a standard concentration used for recording unbiased emission and absorption spectra [41].

$$\text{HHH-}[\text{Cr}(\mathbf{L2})_3]^{3+} + \text{Ln}^{3+} \rightleftharpoons \text{HHH-}[\text{LnCr}(\mathbf{L2})_3]^{6+} \; \beta_{1,1}^{[\text{Cr}(\mathbf{L2})_3],\text{Ln}} \qquad (5)$$

This drawback can be turned into an advantage for chiral resolution because inert and triply-charged HHH-[Cr(**L2**)$_3$]$^{3+}$ complexes are easily prepared and loaded onto an aqueous Sephadex cation-exchange column. Elution with chiral $Na_2Sb_2[(+)\text{-}C_4O_6H_2]_2$ results in two successive spots for the helical enantiomers *M*-$(+)_{589}$-[Cr(**L2**)^3]$^{3+}$ and *P*-$(-)_{589}$-[Cr(**L2**)$_3$]$^{3+}$, which are eventually re-combined with Ln(III) in acetonitrile to give *MM*-[LnCr(**L2**)$_3$]$^{3+}$ and *PP*-[LnCr(**L2**)$_3$]$^{3+}$ (Fig. 11) [36c].

Circular dicrochroism (CD, Fig. 12a) and circularly polarized luminescence (CPL, Fig. 12b) monitored in solution underline the kinetic inertness and the helical nature of these dinuclear Cr–Ln complexes [36c,36d,36f]. Closely related chiral resolution is provided by *M*-[(acac)$_2$Cr(ox)]$^-$, which diastereochemically reacts with Ln^{3+} and [HB(pz)$_3$]$^-$ in water to yield a single diastereomer [*M*-(acac)$_2$Cr(ox)-*P*-Ln(HB(pz)$_3$)$_2$]. NIR-CD and NIR-MCD spectra recorded in dichloromethane solution were used to probe the chiral environments around Ln = Nd, Sm, Dy, Tm and Yb [25b,25c].

The introduction of a second kinetically inert Cr(III) capping unit in the trinuclear helicate [CrLnCr(**L3**)$_3$]$^{9+}$ (Fig. 8b) significantly limits Ln(III)-decomplexation in solution, but it concomitantly introduces some novel difficulties since the large paramagnetic moment precludes the acquisition of exploitable high-resolution NMR spectra for both [Cr^{II}LnCr^{II}(**L3**)$_3$]$^{7+}$ (Fig. 13a) and [Cr^{III}LnCr^{III}(**L3**)$_3$]$^{9+}$ (Fig. 13b). Beyond the crystal structure determination of [Cr^{III}LnCr^{III}(**L3**)$_3$](CF$_3$SO$_3$)$_9$, ESI-MS spectra are the only direct and informative technique suitable for probing the exclusive formation of discrete [CrLnCr(**L3**)$_3$]$^{9+}$ cations in solution (Fig. 10b) [37].

4. Optical sensitization in discrete polynuclear Cr–Ln complexes

Depending on the choice of Ln(III), i.e. depending on the specific electronic structure [Xe]4f^n, n = 0–14, irradiation at the energy of the spin-allowed chromium-centered Cr($^4T_2 \leftarrow {}^4A_2$) transition at 17600 cm^{-1} in [(acac)$_2$Cr(ox)Ln(HB(pz)$_3$)$_2$] results in three different types of optical emission.

(1) With the closed-shell cations Ln = La(III) (4f^0) or Ln = Lu(III) (4f^{14}), only the Cr($^2E \rightarrow {}^4A_2$) phosphorescence can be detected

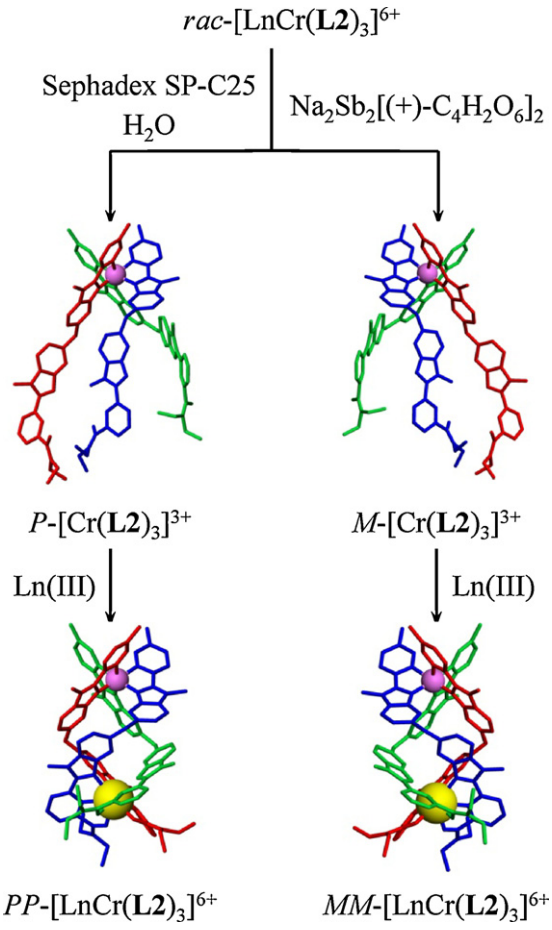

Fig. 11. Resolution of $[Cr(\mathbf{L2})_3]^{3+}$ and synthesis of *PP*-$[LnCr(\mathbf{L2})_3]^{6+}$ and *MM*-$[LnCr(\mathbf{L2})_3]^{6+}$.
Adapted from [36d].

at 12240 cm^{-1} (Ln = La) and 12820 cm^{-1} (Ln = Lu, τ = 0.19 ms at 77 K, Fig. 14) [25a,25d]. Since the ligand-field strength around Cr(III) in $[(acac)_2Cr(ox)Ln(HB(pz)_3)_2]$ is constant along the lanthanide series (Δ = 17600 ± 30 cm^{-1}) [24a], the significant 580 cm^{-1} blue-shift of the energy of the $Cr(^2E)$ level observed for Ln = Lu can be assigned to an increase of the interelectronic Racah parameter (B^{La} = 703 cm^{-1} and B^{Lu} = 746 cm^{-1}, Eq. (4)), corresponding to a decrease in the nephelauxetic effect.

(2) The incorporation of the open-shell cations Ln = Eu(III) ($4f^6$) and Ln = Tb(III) ($4f^8$) partially quenches the Cr-centered phosphorescence without resulting in any Ln-centered luminescence (Fig. 15) [25a]. The broad spectral overlap of the $Cr(^4T_2, {}^2T_2)$ excited levels with $Eu(^5D_0)$ or $Tb(^5D_4)$ simultaneously ensures Cr → Ln energy transfer, which contributes to the partial quenching of Cr-centered luminescence, and Ln → Cr back energy transfers, which is responsible for the complete quenching of Ln-centered emission. Additional phonon-assisted $Cr(^2E) \rightarrow Ln(^7F_j)$ energy transfer contributes to the non-radiative de-excitation of the emissive $Cr(^2E)$ level (Fig. 15).

(3) The introduction of lanthanide acceptors possessing low-energy emissive levels (Ln = Nd, Ho, Er, Tm, Yb) in $[(acac)_2Cr(ox)Ln(HB(pz)_3)_2]$ induces efficient thermally activated $Cr(^2E) \rightarrow$ Ln energy transfer followed by Ln-centered NIR luminescence [25d]. At room temperature, the efficiencies of the $Cr(^2E) \rightarrow$ Ln energy transfer processes is so large that only Ln-centered emissions can be detected. At low temperature, only partial $Cr(^2E) \rightarrow$ Ln energy transfer occurs and both Cr(^{2}E)-centered and Ln-centered luminescence is observed (Fig. 16).

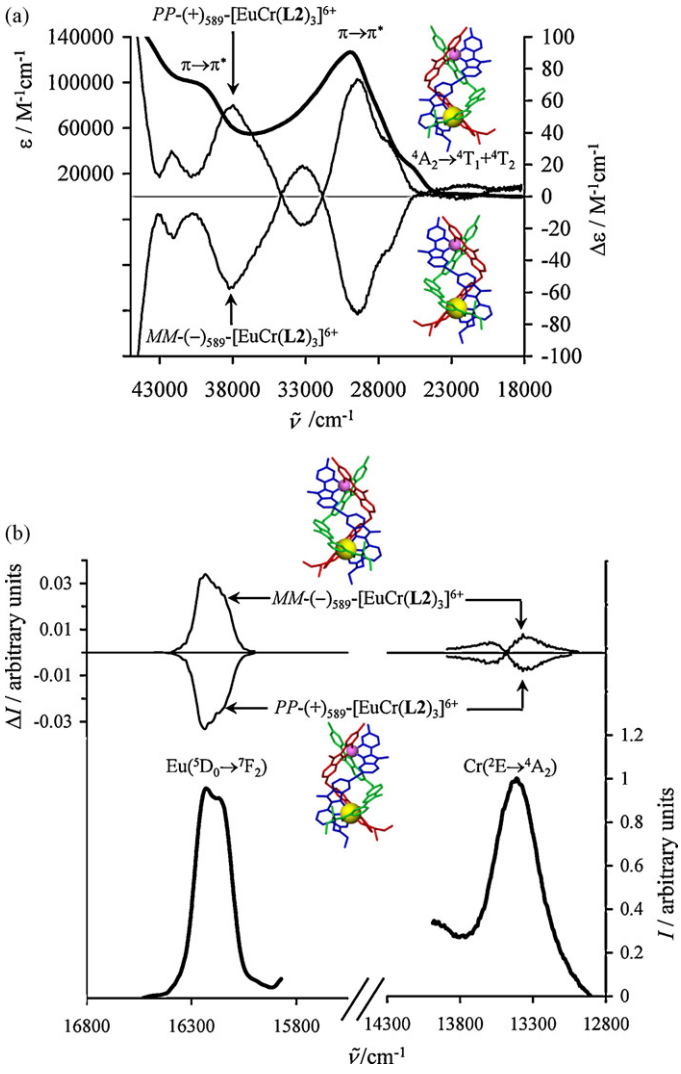

Fig. 12. a) Absorption spectrum of $[EuCr(\mathbf{L2})_3]^{6+}$ (bold line with assignment, 10^{-3} M) and circular dichroism spectra of *MM*-$(-)_{589}$-$[EuCr(\mathbf{L2})_3]^{6+}$ and *PP*-$(+)_{589}$-$[EuCr(\mathbf{L2})_3]^{6+}$ in acetonitrile (5×10^{-5} M, corrected for partial (23%) decomplexation of $[EuCr(\mathbf{L2})_3]^{6+}$). b) Luminescence spectrum of $[EuCr(\mathbf{L2})_3]^{6+}$ (bold line with assignment, 10^{-3} M) and circularly polarized luminescence spectra of *MM*/*PP*-$[EuCr(\mathbf{L2})_3]^{6+}$ in acetonitrile (10^{-3} M, $\tilde{\nu}_{exc}$ = 17, 238 cm^{-1} for $Eu(^5D_0 \rightarrow {}^7F_2)$ and $\tilde{\nu}_{exc}$ = 20, 492 cm^{-1} for $Cr(^2E \rightarrow {}^4A_2)$).
Adapted from [36c].

Closely related optical sensitization behaviors are evidenced for the dinuclear $[LnCr(\mathbf{L2})_3]^{6+}$ helicates. For Ln = La, Gd, Lu, which do not possess energetically accessible excited states for contributing to energy transfer processes, the $Cr(^2E \rightarrow {}^4A_2)$ phosphorescence at 13,300 cm^{-1} (τ = 3.66 ms at 10 K, solid state) is the only luminescence observed in these complexes (Fig. 17a) [36e]. Introducing Δ = 21,000 cm^{-1} [36a] and $\Delta E = E\left[Cr\left(^2E\right)\right] - E\left[Cr\left(^4A_2\right)\right] = 13,300\ cm^{-1}$ observed for $[LnCr(\mathbf{L2})_3]^{6+}$ into Eq. (4) gives $B^{Cr}_{bzimpy} = 747\ cm^{-1}$. Compared with 2,2′-bipyridine in $[Cr(bipy)_3]^{3+}$ (Δ = 23,240 cm^{-1} and $B^{Cr}_{bipy} = 761\ cm^{-1}$, Table 1), we deduce that the didentate 2-pyridyl-benzimidazole (bzimpy) ligand is a weaker σ-donor, but a slightly stronger π-acceptor.

The introduction of visible Eu(III) and Tb(III) emitters into $[LnCr(\mathbf{L2})_3]^{6+}$ opens novel perspectives for molecular

Table 2
Rate constants (k/s^{-1}, Eqs. (6–10)), quantum efficiencies (η, Eq. (11)), intramolecular intermetallic Ln···Cr distances ($R_{D,A}^{Cr,Ln}$/Å) and critical distances for 50% energy transfer ($R_0^{Cr,Ln}$/Å , Eq. (14)) in HHH-[LnCr(**L2**)$_3$]$^{6+}$ and in [CrLnCr(**L3**)$_3$]$^{9+}$ (Ln = Eu, Tb; 10 K) [36,37].

Compd.	k_{lum}^{Cr}	k_{obs}^{Cr}	k_{lum}^{Ln}	k_{obs}^{Ln}	$k_{EnT}^{Ln\rightarrow Cr}$	$\eta_{EnT}^{Ln\rightarrow Cr}$	$R_{D,A}^{Cr,Ln}$	$R_0^{Cr,Ln}$
[GdCr(**L2**)$_3$]$^{6+}$	2.7×10^2	–	–	–	–	–	–	–
[EuZn(**L2**)$_3$]$^{6+}$	–	–	4.0×10^2	–	–	–	8.96	–
[TbZn(**L2**)$_3$]$^{6+}$	–	–	5.3×10^2	–	–	–	–	–
[EuCr(**L2**)$_3$]$^{6+}$	–	3.0×10^2	–	1.8×10^3	1.4×10^3	0.78	9.32	11.5
[TbCr(**L2**)$_3$]$^{6+}$	–	2.9×10^2	–	$>5\times10^4$	$>5\times10^4$	>0.99	–	>20
[CrGdCr(**L3**)$_3$]$^{9+}$	4.4×10^2	–	–	–	–	–	–	–
[ZnEuZn(**L3**)$_3$]$^{9+}$	–	–	5.1×10^2	–	–	–	–	–
[ZnTbZn(**L3**)$_3$]$^{9+}$	–	–	6.5×10^2	–	–	–	–	–
[CrEuCr(**L3**)$_3$]$^{9+}$	–	4.8×10^2	–	5.0×10^3	2.2×10^3	0.90	8.8	12.7
[CrTbCr(**L3**)$_3$]$^{9+}$	–	5.6×10^2	–	$>1.3\times10^5$	$>6.4\times10^4$	>0.99	–	>19

light-conversion since these lanthanides act as donors for the sensitization of Cr(III) phosphorescence (Fig. 17b) [36a].

Modeling the intramolecular Ln → Cr energy transfer processes with the simplified Jablonski diagram shown in Fig. 18a allows the straightforward deduction of the pertinent rate constants (Eqs. (6–10)) and of the energy transfer efficiency (Eq. (11)) from the characteristic excited Ln-centered and Cr-centered lifetimes τ collected within the isostructural series of complexes [LnZn(**L2**)$_3$]$^{5+}$, [GdCr(**L2**)$_3$]$^{6+}$ and [LnCr(**L2**)$_3$]$^{6+}$ (Ln = Eu, Tb, Table 2) [36a].

$$k_{lum}^{Ln} = k_r^{Ln} + k_{nr}^{Ln} = \left(\tau_{LnZn}^{Ln}\right)^{-1} \quad (6)$$

$$k_{lum}^{Cr} = k_r^{Cr} + k_{nr}^{Cr} = \left(\tau_{GdCr}^{Cr}\right)^{-1} \quad (7)$$

$$k_{obs}^{Ln} = \left(\tau_{LnCr}^{Ln}\right)^{-1} \quad (8)$$

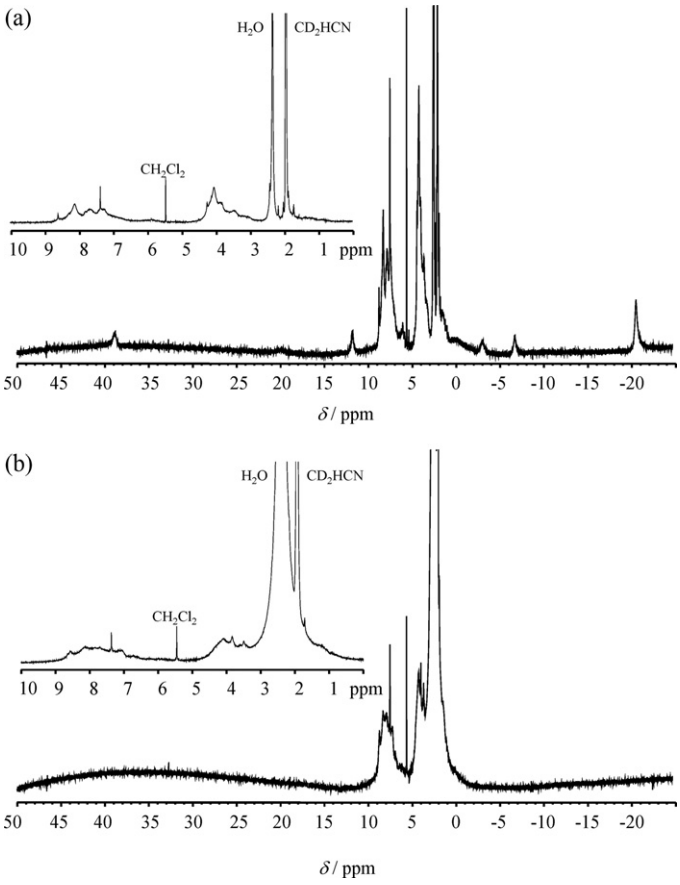

Fig. 13. ^{1}H NMR spectra of a) [$Cr^{II}LaCr^{II}$(**L3**)$_3$]$^{7+}$ and HHH-[$Cr^{III}LaCr^{III}$(**L3**)$_3$]$^{9+}$ in CD_3CN.

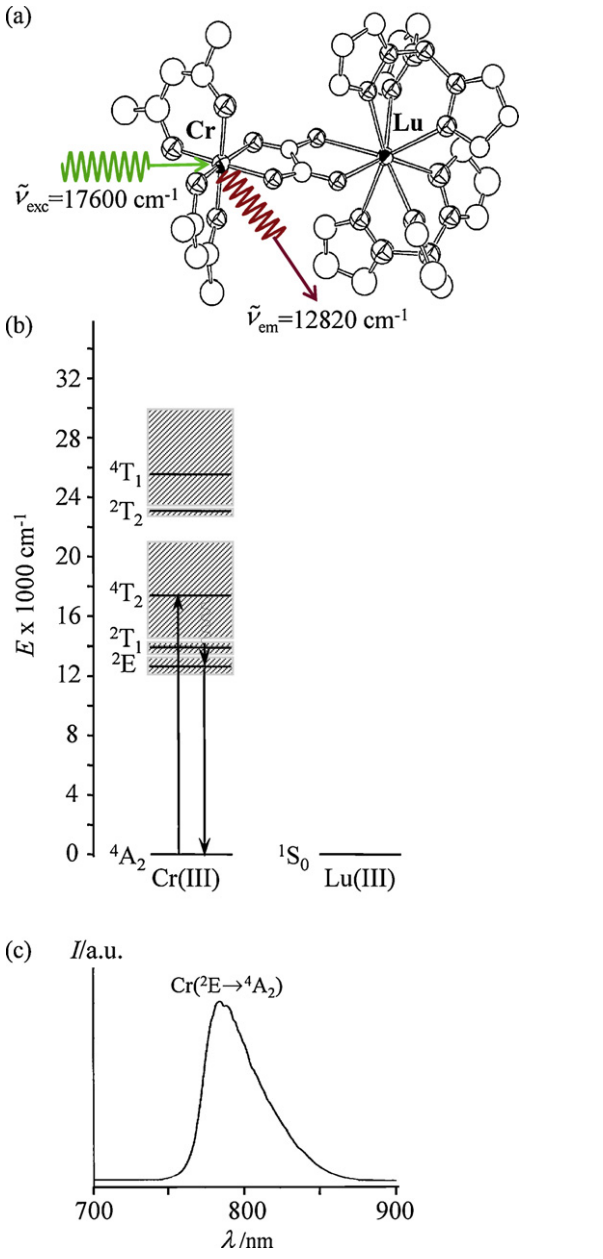

Fig. 14. Optical sensitization occurring in [(acac)$_2$Cr(ox)Lu(HB(pz)$_3$)$_2$]. a) Molecular structure with schematic light-conversion processes, b) Jablonski diagram (straight upward arrow = excitation, undulated arrow = non-radiative multiphonon relaxation and straight downward arrow = luminescence step), and c) emission spectrum [25a].

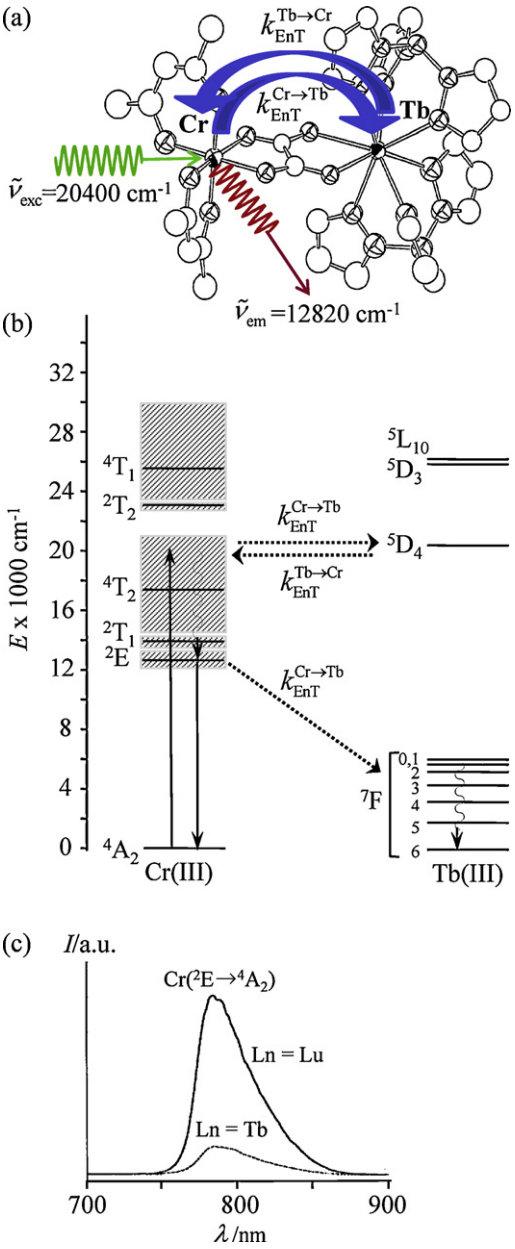

Fig. 15. Optical sensitization occurring in [(acac)$_2$Cr(ox)Tb(HB(pz)$_3$)$_2$]. a) Molecular structure with schematic light-conversion processes, b) Jablonski diagram (straight upward arrow = excitation, dotted arrow = non-radiative energy transfer, undulating arrow = non-radiative multiphonon relaxation and straight downward arrow = luminescence step, and c) emission spectra [25a].

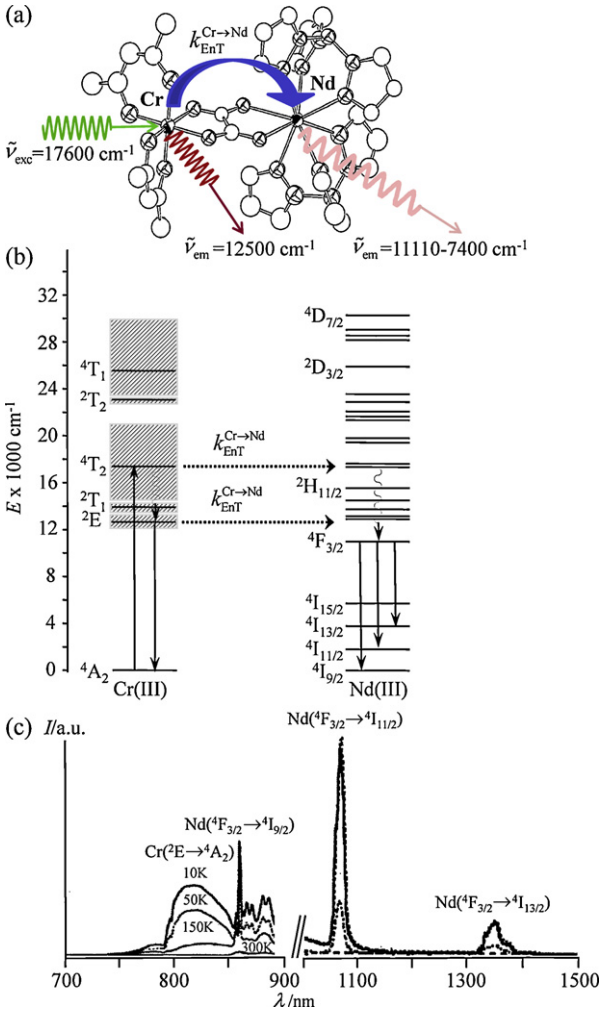

Fig. 16. Optical sensitization occurring in [(acac)$_2$Cr(ox)Nd(HB(pz)$_3$)$_2$]. a) Molecular structure with schematic light-conversion processes, b) Jablonski diagram (straight upward arrows = excitation, dotted arrows = non-radiative energy transfer, undulating arrows = non-radiative multiphonon relaxation and straight downward arrows = luminescence step, and c) emission spectra [25d].

$$k_{obs}^{Cr} = \left(\tau_{LnCr}^{Cr}\right)^{-1} \tag{9}$$

$$k_{EnT}^{Ln\to Cr} = k_{obs}^{Ln} - k_{lum}^{Ln} = \left(\tau_{LnCr}^{Ln}\right)^{-1} - \left(\tau_{LnZn}^{Ln}\right)^{-1} \tag{10}$$

$$\eta_{EnT}^{Ln\to Cr} = \frac{k_{EnT}^{Ln\to Cr}}{k_{EnT}^{Ln\to Cr} + k_{lum}^{Ln}} = 1 - \frac{\tau_{LnCr}^{Ln}}{\tau_{LnZn}^{Ln}} \tag{11}$$

It can be immediately noticed that the rate constants for Eu → Cr or Tb → Cr energy transfers ($k_{EnT}^{Ln\to Cr}$ in Table 2, column 6) favorably compete with intrinsic Ln-centered de-excitation pathways (k_{lum}^{Ln} in Table 2, column 4) leading to considerable energy transfer efficiencies ($0.78 \le \eta_{EnT}^{Ln\to Cr} \le 1.0$) despite Cr···Ln contact distances of about 1 nm in HHH-[LnCr(**L2**)$_3$]$^{6+}$. Though recent investigations [42] suggest that long-distance intermetallic d ↔ f energy transfers may include a competition between the electron-exchange mechanism, which usually requires orbital overlap between closely spaced donor and acceptor components (i.e. Dexter-type [11]), and the (multipolar) coulombic interaction between the donor and acceptor electric fields (i.e. Förster-type [10]), the rate constants collected for HHH-[LnCr(**L2**)$_3$]$^{6+}$ (Ln = Eu, Tb) were analyzed within the strict limit of the long-range electron dipole–dipole formalism [36d]. In these conditions, Eq. (1) becomes [43]:

$$W_{D,A}^{Ln,Cr} \propto k_{EnT}^{Ln\to Cr} = \alpha \frac{Q_A^{Cr}}{n^4 \tau_{r,D}^{Ln} \left(R_{D,A}^{Ln,Cr}\right)^6 \left(\tilde{\nu}_{D,A}^{Ln,Cr}\right)^4} \Omega_{D,A}^{Ln,Cr} = k_{lum,D}^{Ln} \left(\frac{R_0^{Ln,Cr}}{R_{D,A}^{Ln,Cr}}\right)^6 \tag{12}$$

$$\text{with } R_0^{Ln,Cr} = \left(\frac{\alpha Q_A^{Cr} \Omega_{D,A}^{Ln,Cr} \phi_D^{Cr}}{n^4 \left(\tilde{\nu}_{D,A}^{Ln,Cr}\right)^4}\right)^{1/6}$$

Q_A is the integrated absorption cross section of the acceptor transition, $\tau_{r,D}$, $\tau_{lum,D}$ and $\phi_D = \tau_{lum,D}/\tau_{r,D} = \left(k_{lum,D} \cdot \tau_{r,D}\right)^{-1}$ are the radiative, intrinsic lifetimes and luminescence quantum yield of the donor in absence of energy transfer, $R_{D,A}$ is the donor–acceptor distance separation, $\tilde{\nu}_{D,A}$ is the resonance frequency and n is the

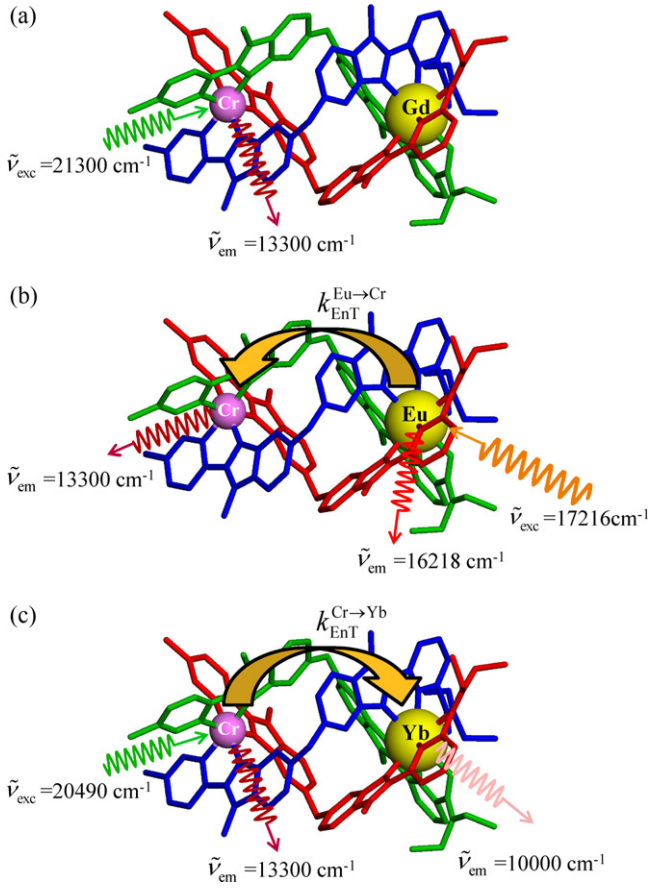

Fig. 17. Molecular structures of $[LnCr(\mathbf{L2})_3]^{6+}$ cations with schematic light-sensitization processes for a) Ln = Gd, b) Ln = Eu and c) Ln = Yb [36].

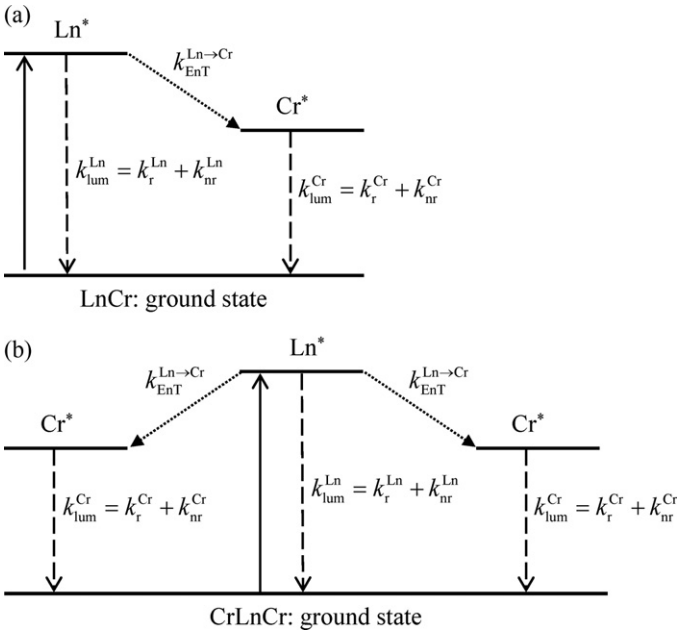

Fig. 18. Simple kinetic models for the de-excitation and Cr ↔ Ln communication in a) HHH-$[LnCr(\mathbf{L2})_3]^{6+}$ and b) $[CrLnCr(\mathbf{L3})_3]^{9+}$ (Ln = Eu, Tb). Straight upward arrows = excitation, dotted arrows = non-radiative energy transfers, and straight downward dashed arrows = radiative + non-radiative decays.

refractive index of the medium separating the donor and the acceptor. α collects fundamental constants and depends on the units used for computing the critical distance R_0 at which $k_{EnT}^{D\rightarrow A} = k_{lum,D}$, and consequently $\eta_{EnT}^{D\rightarrow A} = 0.5$ (Eq. (11)) [43]. Using centimeter units for distances and molar concentrations, Eq. (12) can be converted into Eq. (13) where the resonance frequency $\tilde{\nu}_{D,A}$ and the absorption cross section are partitioned between the spectral overlap integral J_F and a factor κ taking into account the relative orientation of donor and acceptor electric dipoles (generally taken as 2/3 for a randomly oriented system) [6].

$$W_{D,A}^{Ln,Cr} = k_{EnT}^{Ln\rightarrow Cr} = 8.8\times10^{-25}\frac{\left(\kappa^{Cr,Ln}\right)^2\phi_D^{Cr}}{n^4\tau_{lum,D}^{Ln}\left(R_{D,A}^{Ln,Cr}\right)^6}J_F^{Ln,Cr} = k_{lum,D}^{Ln}\left(\frac{R_0^{Ln,Cr}}{R_{D,A}^{Ln,Cr}}\right)^6 \quad (13)$$

$$\text{with } R_0^{Ln,Cr} = \left(\frac{8.8\times10^{-25}\left(\kappa^{Cr,Ln}\right)^2\phi_D^{Cr}}{n^4}J_F\right)^{1/6} \text{ and } J_F = \frac{\int D(\tilde{\nu})A(\tilde{\nu})/\tilde{\nu}^4 d\tilde{\nu}}{\int D(\tilde{\nu})d\tilde{\nu}}$$

D is the emission line shape function for the donor emission, A the absorption coefficient of the acceptor transition. Introducing Eq. (12) or Eq. (13) into Eq. (11) yields

$$\eta_{EnT}^{Ln\rightarrow Cr} = \left[1+\left(\frac{R_{D,A}^{Ln,Cr}}{R_0^{Ln,Cr}}\right)^6\right]^{-1} = \frac{\left(R_0^{Ln,Cr}\right)^6}{\left(R_0^{Ln,Cr}\right)^6+\left(R_{D,A}^{Ln,Cr}\right)^6} \quad (14)$$

Numerical values for the critical distance allowing a 50% energy transfer efficiency $R_0^{Ln,Cr}$ (Table 2, column 9) then simply result from Eq. (14) when pertinent energy transfer efficiencies (Table 2, column 7) operating in HHH-$[LnCr(\mathbf{L2})_3]^{6+}$ are confronted with the intramolecular intermetallic Ln···Cr distances taken as $R_{D,A}^{Ln,Cr}$ (Table 2, column 8).

With $R_0^{Eu,Cr} = 11.5$ Å, and especially $R_0^{Tb,Cr} > 20$ Å, we suspect that superexchange pathways may have non-negligible contributions to $k_{EnT}^{Ln\rightarrow Cr}$, but, whatever the origin of these large apparent values, extended Ln/Cr helicates may be foreseen for the design of molecular directional light-downconverters operating over nanometric distances on the millisecond timescale [36a]. Increasing the temperature from 10 K to 295 K, or working in acetonitrile solution do not strongly affect the Cr–Ln communication in these dinuclear complexes (Fig. 19).

When trivalent lanthanides with low-lying emitting levels (Ln = Nd, Yb) are introduced into HHH-$[LnCr(\mathbf{L2})_3]^{6+}$, the direction of the energy transfer is reversed and Cr(III) acts as a donor for sensitizing Ln(III) (Fig. 17c) [36c,36e]. Eqs. (6–9) still apply, but Eqs. (10–11) are replaced with Eqs. (15–16).

$$k_{EnT}^{Cr\rightarrow Ln} = k_{obs}^{Cr} - k_{lum}^{Cr} = \left(\tau_{LnCr}^{Cr}\right)^{-1} - \left(\tau_{GdCr}^{Cr}\right)^{-1} \quad (15)$$

$$\eta_{EnT}^{Cr\rightarrow Ln} = \frac{k_{EnT}^{Cr\rightarrow Ln}}{k_{EnT}^{Cr\rightarrow Ln}+k_{lum}^{Cr}} = 1 - \frac{\tau_{LnCr}^{Cr}}{\tau_{GdCr}^{Cr}} \quad (16)$$

Modeling the intramolecular Cr → Ln energy transfer processes with the simplified Jablonski diagram shown in Fig. 20a, allows the straightforward deduction of pertinent rate constants (Eqs. (6–9 and 15)) and of the energy transfer efficiencies (Eq. (16)) from the characteristic excited Ln-centered states and Cr-centered lifetimes τ collected within the isostructural series $[LnZn(\mathbf{L2})_3]^{5+}$, $[GdCr(\mathbf{L2})_3]^{6+}$ and $[LnCr(\mathbf{L2})_3]^{6+}$ (Ln = Nd, Yb, Table 3) [36c,36e].

The energy transfer efficiencies $0.46 \le \eta_{EnT}^{Cr\rightarrow Ln} \le 0.87$ are comparable with those found for the reverse situation when Ln(III) = Eu, Tb act as donors for Cr(III), thus leading to similar critical distances for an energy transfer efficiency of 50% ($9\,Å \le R_0^{Ln,Cr} \le 13\,Å$) characterizing the directional Vis → NIR light-conversion processes in

Table 3
Rate constants (k/s^{-1}, Eqs. (6–9) and (15)), efficiencies (η, Eq. (16)), intramolecular intermetallic Ln···Cr distances ($R_{D,A}^{Cr,Ln}$/Å) and critical distances for 50% energy transfer ($R_0^{Cr,Ln}$/Å , Eq. (14)) in HHH-[LnCr(**L2**)$_3$]$^{6+}$ and [CrLnCr(**L3**)$_3$]$^{9+}$ (Ln = Nd, Er, Yb; 10 K) [36,37].

Compd	k_{lum}^{Cr}	k_{obs}^{Cr}	k_{lum}^{Ln}	k_{obs}^{Ln}	$k_{EnT}^{Cr\rightarrow Ln}$	$\eta_{EnT}^{Cr\rightarrow Ln}$	$R_{D,A}^{Cr,Ln}$	$R_0^{Cr,Ln}$
[GdCr(**L2**)$_3$]$^{6+}$	2.7×10^2	–	–	–	–	–	–	–
[NdZn(**L2**)$_3$]$^{6+}$	–	–	6.8×10^5	–	–	–	8.96	–
[YbZn(**L2**)$_3$]$^{6+}$	–	–	5.0×10^4	–	–	–	–	–
[NdCr(**L2**)$_3$]$^{6+}$	–	2.1×10^3	–	2.1×10^3	1.9×10^3	0.87	9.28	12.8
[YbCr(**L2**)$_3$]$^{6+}$	–	5.1×10^2	–	5.1×10^2	2.4×10^2	0.46	9.33	9.1
[CrGdCr(**L3**)$_3$]$^{9+}$	4.4×10^2	–	–	–	–	–	–	–
[ZnNdZn(**L3**)$_3$]$^{9+}$	–	–	6.3×10^5	–	–	–	–	–
[ZnYbZn(**L3**)$_3$]$^{9+}$	–	–	3.2×10^4	–	–	–	–	–
[ZnErZn(**L3**)$_3$]$^{9+}$	–	–	2.2×10^5	–	–	–	–	–
[CrNdCr(**L3**)$_3$]$^{9+}$	–	4.0×10^3	–	2.0×10^3	1.6×10^3	0.78	–	10.9
[CrYbCr(**L3**)$_3$]$^{9+}$	–	7.7×10^2	–	6.9×10^2	2.5×10^2	0.36	8.9	8.1
[CrErCr(**L3**)$_3$]$^{9+}$	–	9.3×10^2	–	6.3×10^2	4.9×10^2	0.53	–	9.0

HHH-[LnCr(**L2**)$_3$]$^{6+}$ (Ln = Nd, Yb) [36e]. Interestingly, the NIR Nd(III) and Yb(III) probes, which usually exhibit microsecond excited state lifetimes, emit within the millisecond range when fed by energy transfer from long-lived Cr(III) [36b]. Let's consider the rate Eqs. (17) and (18), which model the time-dependent evolution of the concentrations $|Cr^*(t)|$ and $|Ln^*(t)|$ of the metals in their excited states after a pulsed excitation of Cr(III) in HHH-[LnCr(**L2**)$_3$]$^{6+}$ (Fig. 20a).

$$\frac{d\left|Cr^*(t)\right|}{dt} = -\left(k_{EnT}^{Cr\rightarrow Ln} + k_{lum}^{Cr}\right)\cdot\left|Cr^*(t)\right| \quad (17)$$

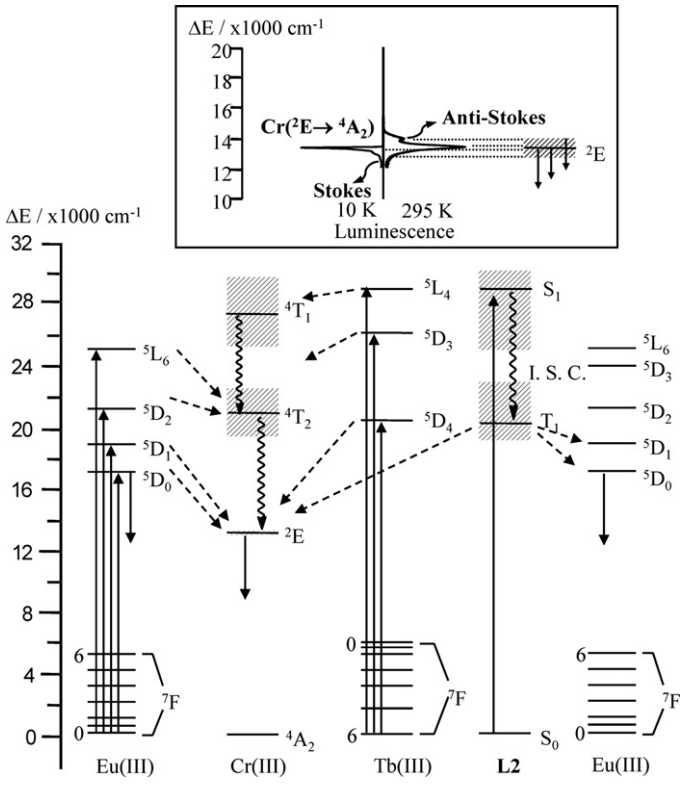

Fig. 19. Partial energy level diagram summarizing the excitation processes (straight upward arrows), energy transfer processes (dotted arrows), non-radiative multi-phonon relaxation (undulating arrows) and radiative emission processes (straight downward arrows) occurring in (HHH)-[LnCr(**L2**)$_3$](CF$_3$SO$_3$)$_6$ (Ln = Eu, Tb). Cr(^{2}T$_1$, ^{2}T$_2$) energy levels are omitted for clarity although they can act as relay for energy transfer processes. The temperature-dependence of the Cr(^{2}E → ^{4}A$_2$) phosphorescence is highlighted.
Adapted from [36a].

$$\frac{d\left|Ln^*(t)\right|}{dt} = k_{EnT}^{Cr\rightarrow Ln}\cdot\left|Cr^*(t)\right| - k_{lum}^{Ln}\left|Ln^*(t)\right| \quad (18)$$

Integration of Eq. (17) is straightforward and yields

$$\left|Cr^*(t)\right| = \left|Cr^*(0)\right|\cdot e^{-\left(k_{EnT}^{Cr\rightarrow Ln}+k_{lum}^{Cr}\right)\cdot t} = \left|Cr^*(0)\right|\cdot e^{-k_{obs}^{Cr}\cdot t} \quad (19)$$

Compared with the intrinsic decay of Cr(III) observed in absence of an acceptor in HHH-[GdCr(**L2**)$_3$]$^{6+}$ ($\left(k_{lum}^{Cr}\right)^{-1} = 3.6$ ms at 10 K), the 46–87% efficiencies of the intramolecular Cr → Ln energy transfers occurring in HHH-[LnCr(L2)$_3$]$^{6+}$ (Ln = Nd, Yb) reduce the Cr(III)-centered excited lifetimes to $\left(k_{obs}^{Cr}\right)^{-1} = 0.5$ ms (NdCr) and 1.9 ms (YbCr, Table 3). Introducing Eq. (19) into Eq. (18) and integration gives [44]

$$\left|Ln^*(t)\right| = \left|Cr^*(0)\right|\cdot\frac{k_{EnT}^{Cr\rightarrow Ln}}{k_{lum}^{Ln}-\left(k_{EnT}^{Cr\rightarrow Ln}+k_{lum}^{Cr}\right)} \times\left(e^{-\left(k_{EnT}^{Cr\rightarrow Ln}+k_{lum}^{Cr}\right)\cdot t} - e^{-k_{Lum}^{Ln}\cdot t}\right) \quad (20)$$

Since $k_{obs}^{Cr} = k_{EnT}^{Cr\rightarrow Ln} + k_{lum}^{Cr} << k_{lum}^{Ln}$, i.e. the residual Cr-centered characteristic excited state lifetime largely exceeds the intrinsic Ln-centered excited state lifetime in HHH-[LnCr(**L2**)$_3$]$^{6+}$ (Ln = Nd, Yb), Eq. (20) reduces to Eq. (21) and the apparent first-order Ln-centered

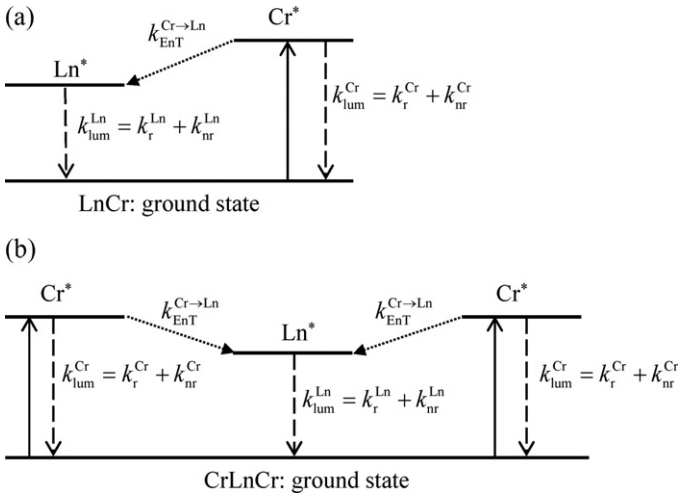

Fig. 20. Simple kinetic models describing the de-excitation and Cr ↔ Ln communication in a) HHH-[LnCr(**L2**)$_3$]$^{6+}$ and b) [CrLnCr(**L3**)$_3$]$^{9+}$ (Ln = Nd, Er, Yb). Straight upward arrows = excitation, dotted arrows = non-radiative energy transfers, and straight downward dashed arrows = radiative + non-radiative decays.

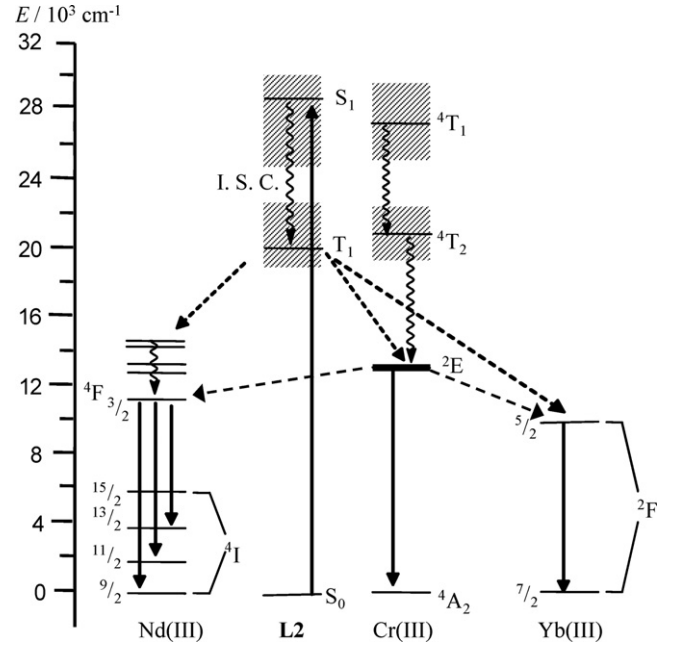

Fig. 21. Partial energy level diagram summarizing the excitation processes (straight upward arrows), energy transfers (dotted arrows), non-radiative multiphonon relaxation (undulating arrows) and radiative emission processes (straight downward arrows) occurring in (HHH)-[LnCr(**L2**)$_3$](CF$_3$SO$_3$)$_6$ (Ln = Nd, Yb). The Cr(^{2}T$_1$, ^{2}T$_2$) levels are omitted for clarity although they can act as relay for energy transfer processes.
Adapted from [36b].

decay rates mirror those of the Cr(III) donor excited states occurring within the millisecond range ($k^{Ln}_{obs} \approx k^{Cr}_{obs}$) [36b,36e].

$$\left|Ln^*(t)\right| = \left|Cr^*(0)\right| \cdot \frac{k^{Cr\rightarrow Ln}_{EnT}}{k^{Ln}_{lum}} \cdot \left(e^{-\left(k^{Cr}_{obs}\right)\cdot t}\right) \quad (21)$$

The mechanisms of the directional Vis → NIR light-sensitization processes occurring in HHH-[LnCr(**L2**)$_3$]$^{6+}$ (Ln = Nd, Yb) are summarized in Fig. 21 [36e].

The connection of a second capping Cr(III) cation in the D$_3$-symmetrical [CrLnCr(**L3**)$_3$]$^{9+}$ helicates complicates the

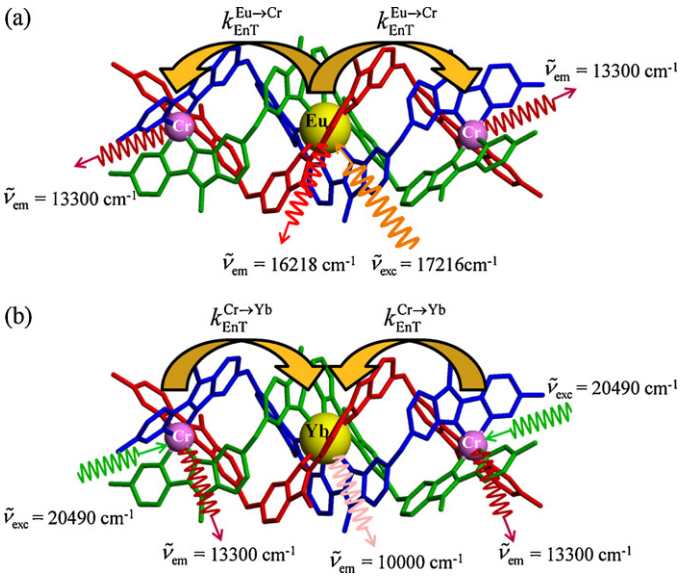

Fig. 22. Molecular structures of [CrLnCr(**L3**)$_3$]$^{9+}$ cations with schematic light-sensitization processes for a) Ln = Eu and b) Ln = Yb [37].

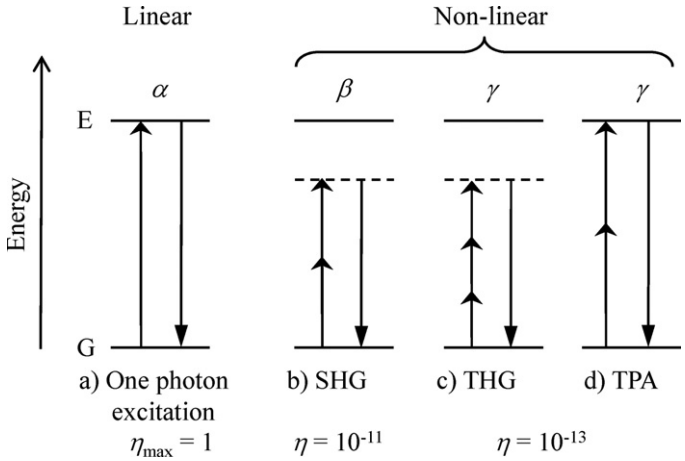

Fig. 23. Energy schemes for a) linear and b)–d) selected non-linear multi-photon processes (G = ground state, E = excited state). a) Resonant one-photon excitation, b) non-resonant second-harmonic generation (SHG), c) non-resonant third-harmonic generation (THG) and d) two-photon absorption (TPA). Relative efficiencies η are normalized for incident flux [52]. Straight upward arrows = excitation processes, straight downward arrows = radiative emission processes.

intramolecular energy transfer schemes with two divergent (Ln = Eu, Tb, Fig. 22a) or two convergent (Ln = Nd, Er, Yb, Fig. 22b) intermetallic energy transfer processes. With Ln = Eu, Tb acting as donors in [CrLnCr(**L3**)$_3$]$^{9+}$, the pertinent rate constants (Fig. 18b) are given in Eqs. (22–26) and the energy transfer efficiency in Eq. (27) (Table 2) [37a].

$$k^{Ln}_{lum} = k^{Ln}_{r} + k^{Ln}_{nr} = \left(\tau^{Ln}_{ZnLnZn}\right)^{-1} \quad (22)$$

$$k^{Cr}_{lum} = k^{Cr}_{r} + k^{Cr}_{nr} = \left(\tau^{Cr}_{CrGdCr}\right)^{-1} \quad (23)$$

$$k^{Ln}_{obs} = \left(\tau^{Ln}_{CrLnCr}\right)^{-1} \quad (24)$$

$$k^{Cr}_{obs} = \left(\tau^{Cr}_{CrLnCr}\right)^{-1} \quad (25)$$

$$k^{Ln\rightarrow Cr}_{EnT} = \frac{\left(k^{Ln}_{obs} - k^{Ln}_{lum}\right)}{2} = \frac{\left[\left(\tau^{Ln}_{CrLnCr}\right)^{-1} - \left(\tau^{Ln}_{CrLnZn}\right)^{-1}\right]}{2} \quad (26)$$

$$\eta^{Ln\rightarrow Cr}_{EnT} = \frac{2k^{Ln\rightarrow Cr}_{EnT}}{2k^{Ln\rightarrow Cr}_{EnT} + k^{Ln}_{lum}} = 1 - \frac{\tau^{Ln}_{CrLnCr}}{\tau^{Ln}_{ZnLnZn}} \quad (27)$$

Compared with HHH-[LnCr(**L2**)$_3$]$^{6+}$, the energy transfer rate constants $k^{Ln\rightarrow Cr}_{EnT}$ in [CrLnCr(**L3**)$_3$]$^{9+}$ are 20–30% larger (Table 2, Ln = Eu, Tb), a phenomenon assigned to an increase in the spectral overlap integral J_F (Eq. (13)) resulting from the replacement of the [Ln(N$_6$O$_3$)] chromophore with [Ln(N$_9$)] (Fig. 8) [37a]. When lanthanide acceptors (Ln = Nd, Er, Yb) are used in [CrLnCr(**L3**)$_3$]$^{9+}$ (Fig. 20b), Eqs. (15) and (16) still hold and the efficiency of the Cr → Nd and Cr → Yb energy transfers are only reduced by approximately 10% in the trinuclear complexes (Table 3). Furthermore, the kinetic condition $k^{Cr}_{obs} << k^{Ln}_{lum}$ still applies and the characteristic Nd-, Er- and Yb-centered NIR luminescence lifetimes mirror the residual Cr-centered emissions (Table 3).

5. Optical upconversion in discrete polynuclear Cr–Ln complexes

The absorption of electromagnetic radiation by a molecule depends on its polarization response $\Delta\mu$ to the alternating electric field E (Eq. (28)) [45].

$$\Delta\mu = \alpha E + \beta E^2 + \gamma E^3 + \ldots \quad (28)$$

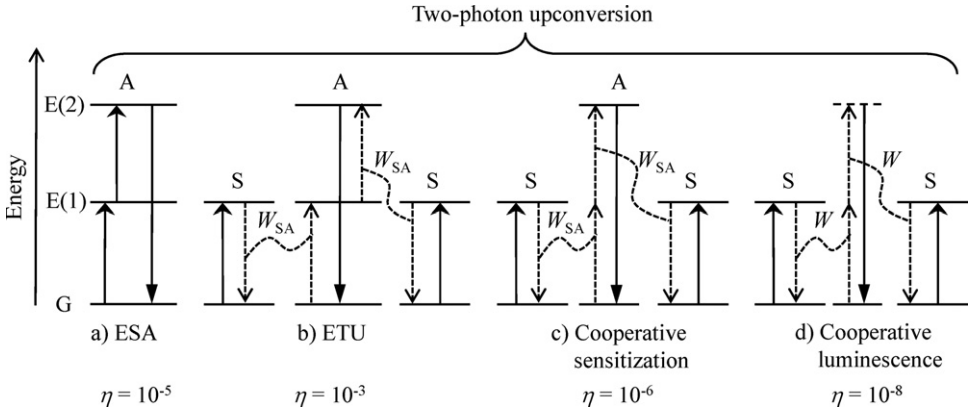

Fig. 24. Energy schemes for selected two-photon upconversion processes (G = ground state, E(1), E(2) = excited states, A = activator, S = sensitizer). A) Excited state absorption (ESA), b) sequential energy transfer upconversion (ETU), c) cooperative sensitization and d) cooperative luminescence. Relative efficiencies η are normalized for incident flux [52]. Straight up arrows = excitation processes, dotted arrows = energy transfer processes. Straight down arrows = luminescence step.

The linear polarizability α belongs to the realm of linear optics. Its real part, Re(α), is involved in the calculation of the refractive index, whereas its imaginary part, Im(α), determines the one-photon extinction coefficients ε responsible for the efficiency of the excitation used for inducing standard sensitization processes (Fig. 23a and Section 4).

β and γ represent the first- and second-order hyperpolarizability terms of ranks 2 and 3, respectively. β quantifies all second-order non-linear optical (NLO) effects such as second-harmonic generation (SHG), a non-resonant multiphoton absorption producing a single emission at double energy during the irradiation (Fig. 23b). γ controls the third-order NLO effects such as third-harmonic generation (THG, Fig. 23c) or two-photon absorption (TPA, Fig. 23d) whose cross section is given by the imaginary part Im(γ). Consequently, any molecule is prone to convert low-energy photons toward higher energy by using its non-linear response to electric polarization, but the efficiencies of these processes are faint (i.e. β, $\gamma \ll \alpha$) and the resulting signals usually lie below instrumental limits of detection except for optimized polarizable systems under high power laser irradiations [46]. To the best of our knowledge, no discrete Cr/Ln polynuclear molecular complex has been investigated for NLO multiphoton absorption.

In 1966, Auzel proposed to consider cases where the emitting ions (often termed the activator: A) are already in an excited state for absorbing an additional photon either from an external irradiation source (excited-state absorption, ESA, Fig. 24a) or from energy transfer involving sensitizer ions, S (Fig. 24b–d) [47]. Since these processes only rely on linear optical processes requiring the successive absorption of two photons leading to the upconverted emission, their efficiencies are approximately 10^3–10^8 larger than for NLO processes. Whereas cooperative sensitization (Fig. 24c) and cooperative luminescence (Fig. 24d) exhibit only very small efficiencies and require close contact distances between the sensitizers and the activators, a situation which is difficult to realize in discrete coordination complexes [48], ESA (Fig. 24a) and sequential energy tranfer upconversion ETU (Fig. 24b) are better suited for attempting to realize upconversion within the frame of molecular processes. However, the efficiency of ESA and ETU processes strongly depends on the characteristic lifetime of the intermediate excited state of the activator (E(1) in Fig. 24). Güdel and coworkers showed that the vibrationally coupled non-radiative relaxation affecting the closely spaced excited states in molecular lanthanide complexes such as $Na_3[Ln(2,6\text{-dipicolinate})_3]$ (Ln = Er, Tm) prevented the detection of luminescence, and gave no opportunity to induce and observe upconversion in these molecular compounds [49]. The use of low-energy phonon solid-state matrices is an obvious remedy for minimizing vibrationally induced non-radiative relaxation and Cr/Yb cooperative sensitization has been reported for several co-doped garnets (Fig. 5) [15,16]. Attempts to reduce the size of the chemical entity responsible for upconversion to nanometric dimensions successfully lead to upconverting nanoparticles based on ionic fluorides or oxides doped with various lanthanides, but we cannot find examples involving molecular Cr/Ln pairs [50]. In order to overcome the molecular limitation found for lanthanide upconversion, we first reconsider the basic rate Eqs. (29) and (30) which model the time-dependent population of the excited stated involved in the ESA mechanism (Fig. 25a). W_A are the rate constants for excitation processes, k_A are the rate constants for decay processes (radiative + non-radiative) and N_A are the population densities.

$$\frac{dN_A^{|1\rangle}}{dt} = W_A^{0\to1}N_A^{|0\rangle} - k_A^1 N_A^{|1\rangle} - W_A^{1\to2}N_A^{|1\rangle} \tag{29}$$

$$\frac{dN_A^{|2\rangle}}{dt} = W_A^{1\to2}N_A^{|1\rangle} - k_A^2 N_A^{|2\rangle} \tag{30}$$

Under continuous-wave irradiation, the pumping rate from a level $|i\rangle$ into a level $|j\rangle$ is given by [51]

$$R_A^{|i\rangle} = W_A^{i\to j}N_A^{|i\rangle} = \frac{\lambda_P}{hc\pi(\omega_P)^2}P\sigma_A^{|i\rangle}N_A^{|i\rangle} = fP\sigma_A^{|i\rangle}N_A^{|i\rangle} \tag{31}$$

with λ_P the pump wavelength, ω_P the pump radius, P the incident pump power, h Planck constant, c the vacuum speed of light, and $\sigma_A^{|i\rangle}N_A^{|i\rangle}$ the absorption cross section of the $|i\rangle$ level for the $i \to j$ transition. Introducing Eq. (31) into Eqs. (29) and (30) yields

$$\frac{dN_A^{|1\rangle}}{dt} = fP\sigma_A^{|0\rangle}N_A^{|0\rangle} - k_A^1 N_A^{|1\rangle} - fP\sigma_A^{|1\rangle}N_A^{|1\rangle} \tag{32}$$

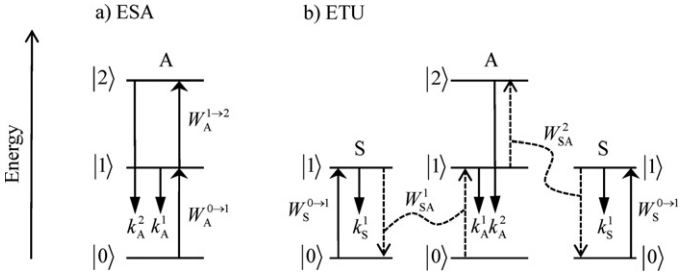

Fig. 25. Simplified three-level upconversion diagrams for a) ESA and b) ETU ($|0\rangle$ = ground state, $|1\rangle$, $|2\rangle$ = excited states, A = activator, S = sensitizer). Straight up arrows = excitation processes, dotted arrows = energy transfers. Straight down arrows = radiative + non-radiative decays.

$$\frac{dN_A^{|2\rangle}}{dt} = fP\sigma_A^{|1\rangle}N_A^{|1\rangle} - k_A^2 N_A^{|2\rangle} \quad (33)$$

Assuming steady-state excitation $dN_A^{|1\rangle}/dt = dN_A^{|2\rangle}/dt = 0$, Eqs. (32) and (33) become

$$fP\sigma_A^{|0\rangle}N_A^{|0\rangle} = k_A^1 N_A^{|1\rangle} + fP\sigma_A^{|1\rangle}N_A^{|1\rangle} \quad (34)$$

$$fP\sigma_A^{|1\rangle}N_A^{|1\rangle} = k_A^2 N_A^{|2\rangle} \quad (35)$$

which can be combined into Eq. (36), in which $N_A^{|0\rangle} \approx N_{tot}$ = constant for a weak incident power.

$$N_A^{|2\rangle}(\mathrm{ESA}) = \frac{f^2\sigma_A^{|0\rangle}\sigma_A^{|1\rangle}P^2N_A^{|0\rangle}}{k_A^2\left(k_A^1 + f\sigma_A^{|1\rangle}P\right)} \quad (36)$$

The same approach applied to the ETU mechanism for a system with a statistical distribution of donors and acceptors, as schematized in Fig. 25b, gives the rate equations [51]

$$\frac{dN_A^{|1\rangle}}{dt} = \left(W_{SA}^1 N_S^{|1\rangle}\right)N_A^{|0\rangle} - k_A^1 N_A^{|1\rangle} - \left(W_{SA}^2 N_S^{|1\rangle}\right)N_A^{|1\rangle} \quad (37)$$

$$\frac{dN_A^{|2\rangle}}{dt} = \left(W_{SA}^2 N_S^{|1\rangle}\right)N_A^{|1\rangle} - k_A^2 N_A^{|2\rangle} \quad (38)$$

$$\frac{dN_S^{|1\rangle}}{dt} = W_S^{0\to1}N_S^{|0\rangle} - k_S^1 N_S^{|1\rangle} - \left(W_{SA}^1 + W_{SA}^2\right)N_S^{|1\rangle} \quad (39)$$

Introducing Eq. (31) into Eq. (39) and taking into account steady-state excitation conditions $dN_A^{|1\rangle}/dt = dN_A^{|2\rangle}/dt = dN_S^{|1\rangle}/dt = 0$, the population densities are given by

$$N_A^{|1\rangle} = \frac{W_{SA}^1 N_S^{|1\rangle}N_A^{|0\rangle}}{k_A^1 + W_{SA}^2 N_S^{|1\rangle}} \quad (40)$$

$$N_A^{|2\rangle} = \frac{W_{SA}^2 N_S^{|1\rangle}N_A^{|1\rangle}}{k_A^2} \quad (41)$$

$$N_S^{|1\rangle} = \frac{f\sigma_S^{|0\rangle}P\,N_S^{|0\rangle}}{W_{SA}^1 + W_{SA}^2 + k_S^1} \quad (42)$$

The introduction of Eqs. (40) and (42) into Eq. (41) followed by algebraic transformations eventually yield

$$N_A^{|2\rangle}(\mathrm{ETU}) = \frac{f^2\left(\sigma_S^{|0\rangle}\right)^2P^2N_A^{|0\rangle}W_{SA}^1W_{SA}^2\left(N_S^{|0\rangle}\right)^2}{k_A^2\left(W_{SA}^1 + W_{SA}^2 + k_S^1\right)\left(k_A^1\left(W_{SA}^1 + W_{SA}^2 + k_S^1\right) + f\sigma_S^{|0\rangle}PW_{SA}^2N_S^{|0\rangle}\right)} \quad (43)$$

Again, $N_S^{|0\rangle} \approx N_{tot}$ = constant only for a weak incident power.

Comparing Eqs (43) and (36) shows that the numerator of the ETU mechanism gains over single chromophore ESA by the product $W_{SA}^1W_{SA}^2\left(N_S^{|0\rangle}\right)^2$. Moreover, $N_A^{|2\rangle}$(ETU) has no extremum for $W_{SA} > 0$ and strictly grows with increasing energy transfer rate constant W_{SA}, so that the product $W_{SA}^1W_{SA}^2$ should be as large as possible [52]. Chemically speaking, $W_{SA}^1W_{SA}^2$ can be optimized with efficient S→A energy transfer couples, while $\left(N_S^{|0\rangle}\right)^2$ is maximized by a high local concentration of sensitizers around the activator. We also note that the product of the absorption cross sections of the activator $\sigma_A^{|0\rangle}\sigma_A^{|1\rangle}$ in the ESA mechanism (Eq. (36)) is replaced with $\left(\sigma_S^{|0\rangle}\right)^2$ in the ETU mechanism. Finally, the sum $W_{SA}^1 + W_{SA}^2 + k_S^1$ contributes twice to the denominator and should be minimized for providing maximum ETU efficiency. Altogether, the ETU mechanism can be optimized in a molecular system made up of a maximum number of sensitizers ($\left(N_S^{|0\rangle}\right)^2$ is large) possessing a high absorption cross section ($\left(\sigma_S^{|0\rangle}\right)^2$ is large), a long characteristic excited lifetime (k_S^1 is small), and located at distances from the activator, for which the energy transfer rate constants are considerable ($W_{SA}^1W_{SA}^2$ is large). With this consideration in mind, the trinuclear complex $[CrErCr(\mathbf{L3})_3]^{9+}$ is an appealing candidate since two long-lived Cr(III) chromophores ($\tau_{lum}^{Cr} = \left(k_{lum}^{Cr}\right)^{-1} = 2.3$ ms at 10 K in the solid state, Table 3) with small but non-negligible absorption cross section characteristic of d–d transitions are able to generate significant energy transfer processes toward the central Er(III) activator ($\eta_{EnT}^{Cr\to Er} = 53\%$, Table 3, Fig. 26a). Furthermore, the strong ligand-field strength found around Cr(III) in $[CrLnCr(\mathbf{L3})_3]^{9+}$ ($\Delta = 20980\,cm^{-1}$, $B = 748\,cm^{-1}$) ensures a large energy gap $E(Cr(^4T_2))$-$E(Cr(^2E)) = 7600\,cm^{-1}$ which translates into a transparent 20,000–14,000 cm^{-1} window for the potential upconverted green $Er(^4S_{3/2} \to {}^4I_{15/2})$ luminescence expected around 18,400 cm^{-1} (Fig. 26a) [37b]. Irradiation in the spin-allowed ligand-centered $\pi \to \pi^*$ transitions (28,170 cm^{-1}) in $[CrErCr(\mathbf{L3})_3]^{9+}$ confirms the latter assumption since rapid **L3** → Cr(III) and **L3** → Er(III) energy transfer processes eventually lead to rich mixed ligand-centered and metal-centered emission

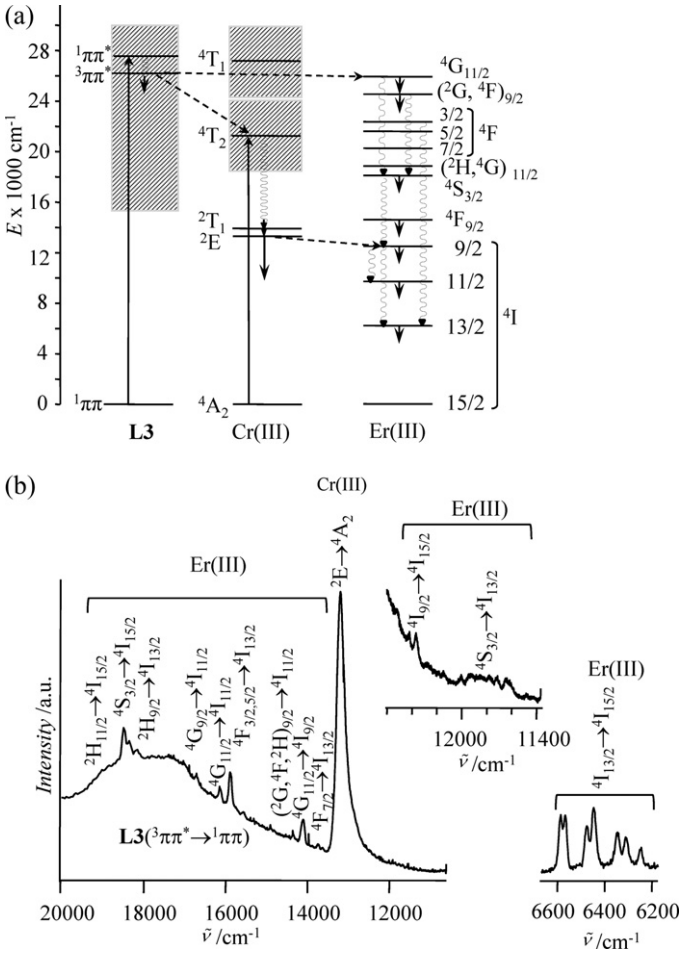

Fig. 26. a) Jablonski diagrams representing the different chromophores in $[CrErCr(\mathbf{L3})_3]^{9+}$ showing the linear luminescence (excitation = straight up arrows, internal conversion = curled arrows, energy transfer = dotted arrows, emission = straight down arrows), and b) emission spectrum of $[CrErCr(\mathbf{L3})_3]^{9+}$ recorded upon ligand-centered excitation (solid state, $\nu_{exc} = 28,170\,cm^{-1}$, 3.5 K). Adapted from [37b].

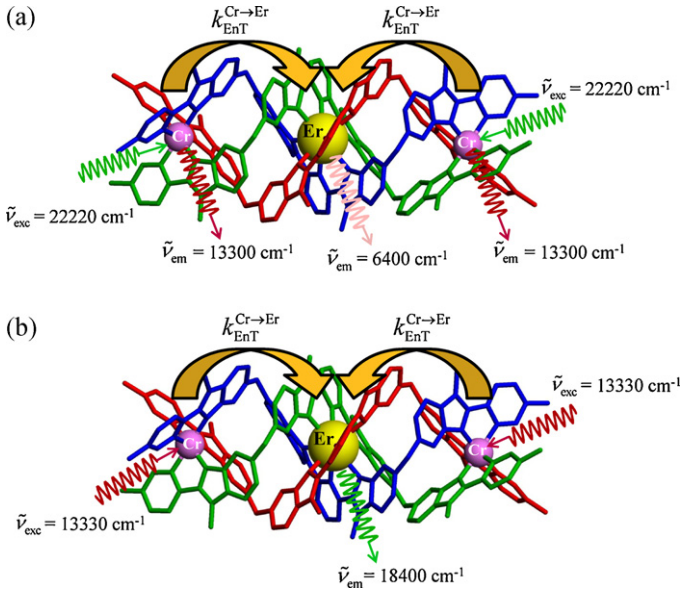

Fig. 27. Molecular structures of $[CrErCr(\mathbf{L3})_3]^{9+}$ cations with schematic a) light-sensitization and b) light-upconversion processes.

bands, among which the $Er(^4S_{3/2} \rightarrow {}^4I_{15/2})$ emission can be detected (Fig. 26b).

Upon selective excitation of the spin-allowed $Cr(^4T_2 \leftarrow {}^4A_2)$ transition at 22,220 cm^{-1}, intersystem crossing and internal conversion rapidly feed the $Cr(^2E)$ level which simultaneously induces $Cr(^2E \rightarrow {}^4A_2)$ phosphorescence at 13,380 cm^{-1} and $Cr(^2E) \rightarrow Er(^4I_{9/2})$ energy transfer ($\eta_{EnT}^{Cr\rightarrow Er} = 53\%$) followed by Er-centered luminescence at 6400 cm^{-1} $Er(^4I_{13/2} \rightarrow {}^4I_{15/2})$ (Fig. 27a).

Selective irradiation of the $Cr(^2E \leftarrow {}^4A_2)$ transition at 13,330 cm^{-1} with a tuneable Ti-sapphire laser indeed produces upconversion luminescence (Fig. 27b) with the detection of the characteristic $Er(^4S_{3/2} \rightarrow {}^4I_{15/2})$ green luminescence at 18,400 cm^{-1} for solid-state samples (Fig. 28a) and for diluted frozen acetonitrile solutions (Fig. 28b) [37b]. Although specific rate equations have to be derived for satisfyingly modeling ETU processes occuring in discrete trinuclear $[CrErCr(\mathbf{L3})_3]^{9+}$ complexes (Fig. 29), the exact quadratic dependence of the photoluminescence intensity on the incident laser power observed in frozen solution ($I \propto P^2$, Fig. 28) implies that $k_A^1\left(W_{SA}^1 + W_{SA}^2 + k_S^1\right) >> f\sigma_S^{|0\rangle} P W_{SA}^2 N_S^{|0\rangle}$ within the frame of the statistical approach [51]. Eq. (43) therefore reduces to

$$N_A^{|2\rangle}(\mathrm{ETU}) \approx \frac{f^2\left(\sigma_S^{|0\rangle}\right)^2 N_A^{|0\rangle} W_{SA}^1 \left(N_S^{|0\rangle}\right)^2}{k_A^2 k_A^1 \left(W_{SA}^1 + W_{SA}^2 + k_S^1\right)^2} P^2 \qquad (44)$$

In other words, the linear decay k_A^1 is the dominant depletion mechanism of the intermediate activator excited state $|1\rangle_A$, whereas the upconversion term $W_{SA}^2 N_S^{|1\rangle}$ becomes negligible ($k_A^1 >> W_{SA}^2 N_S^{|1\rangle}$ in Eq. (40)). This situation is characteristic for a molecular system possessing high-energy oscillators which

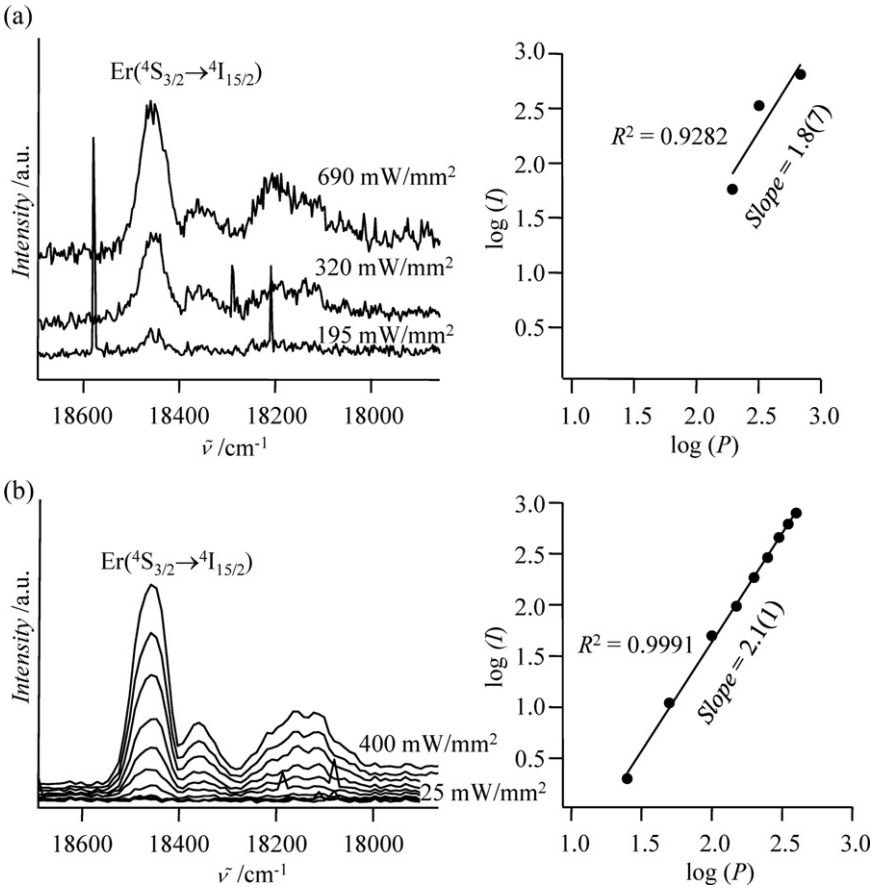

Fig. 28. Green upconversion luminescence in $[CrErCr(\mathbf{L3})_3]^{9+}$ obtained upon irradiation of the $Cr(^2E \leftarrow {}^4A_2)$ transition at varying laser powers: a) solid state (4 K, ν_{exc} = 13, 333 cm^{-1}) and b) 10 mM in acetonitrile (ν_{exc} = 13, 360 cm^{-1}, 30.6 K).

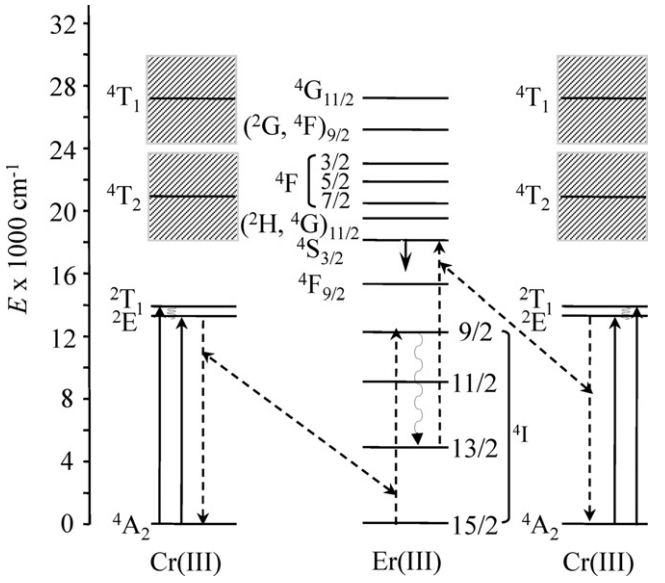

Fig. 29. Jablonski diagrams for the different chromophores in $[CrErCr(\mathbf{L3})_3]^{9+}$ showing the proposed ETU mechanism for linear upconversion luminescence (excitation = straight up arrows, internal conversion = curled arrows, energy transfer = dotted arrows, emission = straight down arrows).
Adapted from [37b] and [53].

efficiently deactivate the closely spaced excited states of the Er(III) activator [49].

It is worth stressing here that the quadratic dependence $I \propto P^2$ found for the $Er(^4S_{3/2} \rightarrow {}^4I_{15/2})$ green upconversion luminescence in $[CrErCr(\mathbf{L3})_3]^{9+}$ has no relationship with the usual signature of second-order non-linear optical response, but it explains why upconversion is sometimes (erroneously) referred to as a NLO process. For being convinced, let's consider the alternative limiting case, for which the linear decay of the intermediate activator excited state $|1\rangle_A$ can be neglected because the upconversion is dominant ($k_A^1 << W_{SA}^2 N_S^{|1\rangle}$ in Eq. (40)). In these conditions, Eq. (43) reduces to

$$N_A^{|2\rangle}(\mathrm{ETU}) = \frac{f\sigma_A^{|0\rangle} N_A^{|0\rangle} W_{SA}^1 N_S^{|0\rangle}}{k_A^2 \left(W_{SA}^1 + W_{SA}^2 + k_S^1\right)} P \qquad (45)$$

and the intensity of the upconversion luminescence depends linearly on the incident laser power, as for any linear optical processes.

6. Conclusions and perspectives

Due to its kinetic inertness, Cr(III) has been considered since the mid-fifties as an ideal cation in mononuclear complexes for investigating ligand-exchange mechanisms, stereochemistry, and for correlating structural parameters with electronic, magnetic and optical properties. However, discrete polynuclear heterometallic d–d [54] or d–f [24–26,36,37] complexes including Cr(III) cations remain scarce in the literature because of the difficult selective incorporation of the different metals in the same (supra)molecular architecture. The use of a pre-formed inert pseudo-octahedral Cr(III) complexes acting as ligand for cascade complexation reactions with additional d-block and/or f-block partners is by far the most popular strategy, but the alternative exploitation of the toolbox of self-assembly with labile Cr(II) analogues followed by oxidative post-modification offers novel perspectives for the preparation of sophisticated discrete polynuclear architectures. A large part of the disaffection for introducing Cr(III) in (supra)molecular heterometallic complexes also comes from its slow-relaxing paramagnetic $Cr(^4A_2)$ ground state, which precludes the use of high-resolution NMR for its characterization. In this context, geometrically analogous fast-relaxing Cr(II) precursors may greatly help for recording parent high-resolution NMR spectra, but ESI-MS remains the most accessible analytical spectroscopic technique for a rapid identification of the different charged Cr(III) complexes present in solution. The pairing of Cr(III) with trivalent lanthanides displays limited magnetic interest because of the weak 3d–4f coupling schemes and of the poor magnetic anisotropy of Cr(III) [24,25,55]. On the contrary, isolated Cr/Ln systems exhibit fascinating optical properties, which benefit from rich metal-centered absorption and emission properties combined with novel functions resulting from tuneable Cr ↔ Ln energy transfers. Depending on the choice of accessible excited spectroscopic levels in the Ln(III) partner, Cr(III) can act as an acceptor (Ln = Eu, Tb) or as a donor (Ln = Nd, Sm, Ho, Dy, Er, Tm, Yb) for directional light-sensitization in dinuclear and trinuclear complexes. Assuming simple dipole-dipolar Förster mechanisms, the critical distances required for a 50% energy transfer efficiency in Cr/Ln pairs fall within the nanometric range, which allows their molecular tuning at the (supra)molecular level and the control of the excited lifetimes of NIR lanthanide emitters by long-lived Cr(III) donors. Last, but not least, the strong-field $[Cr(III)N_6]$ chromophores found in $[CrLnCr(\mathbf{L3})_3]^{9+}$ have been successfully used as sensitizers for the first light-upconversion process performed in discrete coordination complexes. Whereas light-sensitization based on Cr(III)/Ln(III) complexes will probably remain an academic curiosity compared with other more efficient and accessible d–f pairs [20], there is no doubt that the strict quadratic dependence of the intensity of the green upconverted $Er(^4S_{3/2} \rightarrow {}^4I_{15/2})$ luminescence in $[CrLnCr(\mathbf{L3})_3]^{9+}$ on the incident power of the optical source will attract a strong interest for the further design of improved molecular systems in which the upconversion process is optimized with respect to the linear decay of the intermediate excited state of the activator. This unique advantage could lead in the future to the creation of upconverting edifices suitable for novel photonics applications.

Acknowledgements

This work is supported through grants from the Swiss National Science Foundation. S.P. thanks "La Ligue contre le Cancer", Institut National de la Santé et de la Recherche Médicale (INSERM) for financial support in France. The work in France was carried out within the European COST action D38.

References

[1] (a) V.S. Sastri, J.-C.G. Bünzli, C.V.S. Rayudu, J.R. Perumareddi, Modern Aspects of Rare Earths and Their Complexes, Elsevier, Amsterdam, 2003, chapter 8;
(b) G. Liu, B. Jacquier (Eds.), Spectroscopic Properties of Rare Earths in Optical Materials, Spinger-Verlag, Berlin, Heidelberg, 2005;
(c) S. Cotton, Lanthanide and Actinide Chemistry, John Wiley & Sons Ltd, Chichester, 2006.
[2] W.T. Carnall, G.L. Goodman, K. Rajnak, R.S. Sana, J. Chem. Phys. 90 (1989) 3443, Depending on the material and experimental conditions, other levels may also be emissive.
[3] (a) A.D. Kirk, Chem. Rev. 99 (1999) 1607;
(b) P.S. Wagenknecht, P.C. Ford, Coord. Chem. Rev. 255 (2011) 591.
[4] Y. Shen, T. Riedener, K.L. Bray, Phys. Rev. B 61 (2000) 11460.
[5] (a) N. Serpone, M.Z. Hoffman, J. Chem. Educ. 60 (1983) 853;
(b) A. Hauser, M. Mäder, W.T. Robinson, R. Murugesan, J. Ferguson Inorg. Chem. 26 (1987) 1331;
(c) T. Schönherr, M. Atanasov, A. Hauser, Inorg. Chem. 35 (1996) 2077.
[6] (a) T. Lazarides, G.M. Davies, H. Adams, C. Sabatini, F. Barigelletti, A. Barbieri, S.J.A. Pope, S. Faulkner, M.D. Ward, Photochem. Photobiol. Sci. 6 (2007) 1152;
(b) M.D. Ward, Coord. Chem. Rev 254 (2010) 2634.
[7] (a) R.T. Walters, A.W. Adamson, Acta Chem. Scand. A33 (1979) 53;
(b) N.J. Linck, S.J. Berens, D. Magde, R.G. Linck, J. Phys. Chem. 87 (1983) 1733.

[8] R.B. Lessard, M.J. Heeg, T. Buranda, M.W. Perkovic, C.L. Schwarz, Y. Rudang, J.F. Endicott, Inorg. Chem. 31 (1992) 3091.
[9] (a) B. Henderson, G.F. Imbush, Optical Spectroscopy of Inorganic Solids, Clarendon Press, Oxford, 1989;
(b) G. Blasse, B.C. Gramaier, Luminescent Materials, Springer-Verlag, Berlin, 1994.
[10] (a) T. Förster, Ann. Phys. 2 (1948) 55;
(b) T. Förster, Discuss. Faraday Soc. 27 (1959) 7.
[11] D.L. Dexter, J. Chem. Phys. 21 (1953) 836.
[12] P.A. Brayshaw, J.-C.G. Bünzli, P. Froidevaux, J.M. Harrowfield, Y. Kim, A.N. Sobolev, Inorg. Chem. 34 (1995) 2068.
[13] C.K. Ryu, J.F. Endicott, Inorg. Chem. 27 (1988) 2203.
[14] (a) H. Witzke, Theoret. Chim. Acta 20 (1971) 171;
(b) A.B.P. Lever, Inorganic Electronic Spectroscopy, 2nd ed., Elsevier, Amsterdam, The Netherlands, 1984;
(c) A. Trueba, P. Garcia-Fernandez, J.M. Garcia-Lastra, J.A. Aeramburu, M.T. Barriuso, M. Moreno, J. Phys. Chem. A 115 (2011) 1423.
[15] S. Heer, M. Wermuth, K. Krämer, D. Ehrentraut, H.U. Güdel, J. Lumin. 94–95 (2001) 337.
[16] S. Heer, K. Petermann, H.U. Güdel, J. Lumin. 102–103 (2003) 144.
[17] (a) R.G. Wilkins, Kinetics and Mechanisms of Reaction of Transition Metal Complexes, 2nd ed., VCH, Weinheim–New York–Basel–Cambridge, 1991, p. 201;
(b) S.F. Lincoln, A.E. Merbach, Adv. Inorg. Chem. 42 (1995) 1;
(c) S.F. Lincoln, Helv. Chim. Acta 88 (2005) 523;
(d) D.T. Richens, Chem. Rev. 105 (2005) 1961;
(e) L. Helm, A.E. Merbach, Chem. Rev. 105 (2005) 1923.
[18] S. Decurtins, M. Gross, H.W. Schmalle, S. Ferlay, Inorg. Chem. 37 (1998) 2443.
[19] X. Zhang, Y. Cui, F. Zheng, J. Huang, Chem. Lett. 28 (1999) 1111.
[20] (a) M.D. Ward, Coord. Chem. Rev. 251 (2007) 1663;
(b) F.-F. Chen, Z.-Q. Chen, Z.-Q. Bian, C.-H. Huang, Coord. Chem. Rev. 254 (2010) 991.
[21] K.F. Purcell, J.C. Kotz, Inorganic Chemistry, W. B. Saunders Company, Philadelphia–London–Toronto, 1977, chapter 14.
[22] F. Benetollo, G. Bombieri, P. Gilli, P.M. Harlow, A. Polo, L.M. Vallarino, Polyhedron 14 (1995) 2255.
[23] P.A. Brayshaw, A.K. Hall, W.T.A. Harrison, J.M. Harrowfield, D. Pearce, T.M. Shand, B.W. Skelton, C.R. Whitaker, A.H. White, Eur. J. Inorg. Chem. (2005) 1127.
[24] H.-Z. Kou, K.-Q. Hu, H.-Y. Zhao, J. Tang, A.-L. Cui, Chem. Commun. 46 (2010) 6533.
[25] (a) T. Sanada, T. Suzuki, T. Yoshida, S. Kaizaki, Inorg. Chem. 37 (1998) 4712;
(b) M.A. Subhan, T. Suzuki, S. Kaizaki, J. Chem. Soc., Dalton Trans. (2001) 492;
(c) M.A. Subhan, T. Suzuki, S. Kaizaki, J. Chem. Soc., Dalton Trans. (2002) 1416;
(d) M.A. Subhan, H. Nakata, T. Suzuki, J.-H. Choi, S. Kaizaki, J. Lumin. 101 (2003) 307.
[26] (a) R. Kawahata, T. Tsukuda, T. Yagi, M.A. Subhan, H. Nakata, A. Fuyuhiro, S. Kaizaki, Chem. Lett. 32 (2003) 1084;
(b) R. Kawahata, T. Tsukuda, T. Yagi, A. Fuyuhiro, S. Kaizaki, J. Alloys Compd. 408–412 (2006) 976.
[27] J.-D. Compain, P. Mialane, A. Dolbecq, I.M. Mbomekallé, J. Marrot, F. Sécheresse, C. Duboc, E. Rivière, Inorg. Chem. 49 (2010) 2851.
[28] A.B. Yusov, M. Yin, A.M. Fedossev, G.B. Andreev, I.B. Shirokova, J.-C. Krupa, J. Alloys Compd. 344 (2002) 289.
[29] (a) J. Xu, K.N. Raymond, Angew. Chem. Int. Ed. 39 (2000) 2745;
(b) K. Zeckert, J. Hamacek, J.-P. Rivera, S. Floquet, A. Pinto, M. Borkovec, C. Piguet, J. Am. Chem. Soc. 126 (2004) 11589;
(c) X.-Y. Chen, Y. Bretonnière, J. Pécaut, D. Imbert, J.-C.G. Bünzli, M. Mazzanti, Inorg. Chem. 46 (2007) 625;
(d) J. Hamacek, G. Bernardinelli, Y. Filinchuk, Eur. J. Inorg. Chem. (2008) 3419;
(e) C.M.G. dos Santos, A.J. Harte, S.J. Quinn, T. Gunnlaugsson, Coord. Chem. Rev. 252 (2008) 2512;
(f) T. Nabeshima, Bull. Chem. Soc. Jpn. 83 (2010) 969;
(g) B. El Aroussi, S. Zebret, C. Besnard, P. Perrottet, J. Hamacek, J. Am. Chem. Soc. 133 (2011) 10764.
[30] C. Piguet, M. Borkovec, J. Hamacek, K. Zeckert, Coord. Chem. Rev. 249 (2005) 705.
[31] S. Torelli, S. Delahaye, A. Hauser, G. Bernardinelli, C. Piguet, Chem. Eur. J. 10 (2004) 3503.
[32] T. Riis-Johannessen, N. Dupont, G. Canard, G. Bernardinelli, A. Hauser, C. Piguet, Dalton Trans. (2008) 3661.
[33] S. Rigault, C. Piguet, G. Bernardinelli, G. Hopfgartner, Angew. Chem. Int. Ed. Engl. 37 (1998) 169.
[34] L. Chong, R.B. Jordan, Inorg. Chem. 26 (1987) 3855.
[35] B.R. Baker, B.D. Mehta, Inorg. Chem. 4 (1965) 848.
[36] (a) M. Cantuel, G. Bernardinelli, D. Imbert, J.-C.G. Bünzli, G. Hopfgartner, C. Piguet, J. Chem. Soc., Dalton Trans. (2002) 1929;
(b) D. Imbert, M. Cantuel, J.-C.G. Bünzli, G. Bernardinelli, C. Piguet, J. Am. Chem. Soc. 125 (2003) 15698;
(c) M. Cantuel, G. Bernardinelli, G. Muller, J.P. Riehl, C. Piguet, Inorg. Chem. 43 (2004) 1840;
(d) S.G. Telfer, N. Tajima, R. Kuroda, M. Cantuel, C. Piguet, Inorg. Chem. 43 (2004) 5302;
(e) S. Torelli, D. Imbert, M. Cantuel, G. Bernardinelli, S. Delahaye, A. Hauser, J.-C.G. Bünzli, C. Piguet, Chem. Eur. J. 11 (2005) 3228;
(f) P. Gawryszewska, J. Legendziewicz, Z. Ciunik, N. Esfandiari, G. Muller, C. Piguet, M. Cantuel, J.P. Riehl, Chirality 18 (2006) 406.
[37] (a) M. Cantuel, F. Gumy, J.-C.G. Bünzli, C. Piguet, Dalton Trans. (2006) 2647;
(b) L. Aboshyan-Sorgho, C. Besnard, P. Pattison, K.R. Kittilstved, A. Aebischer, J.-C.G. Bünzli, A. Hauser, C. Piguet, Angew. Chem. Int. Ed. 50 (2011) 4108.
[38] (a) I. Bertini, C. Luchinat, Coord. Chem. Rev. 150 (1996) 77;
(b) I. Bertini, M. Fragai, C. Luchinat, G. Parigi, Inorg. Chem. 40 (2001) 4030.
[39] (a) G.N. La Mar, G.R. Van Hecke, J. Chem. Phys. 52 (1970) 5676;
(b) C.C. Scarborough, S. Sproules, T. Weyhermueller, S. DeBeer, K. Wieghardt, Inorg. Chem 50 (2011) 12446.
[40] G.N. La Mar, G.R. Van Hecke, J. Am. Chem. Soc. 91 (1969) 3442.
[41] G. Canard, C. Piguet, Inorg. Chem. 46 (2007) 3511.
[42] T. Lazarides, D. Sykes, S. Faulkner, A. Barbieri, M.D. Ward, Chem. Eur. J. 14 (2008) 9389.
[43] (a) G. Blasse, Phillips Res. Rep. 24 (1969) 131;
(b) V.S. Langford, M.E. von Arx, A. Hauser, J. Phys. Chem. A 103 (1999) 7161.
[44] M.E. Starzak, Mathematical Methods in Chemistry and Physics, Plenum Press, New York and London, 1989, p. 301.
[45] P.N. Prasad, D.J. Williams, Introduction to Nonlinear Optical Effects in Molecules and Polymers, John Wiley & Sons Inc, New York, 1991.
[46] C. Andraud, O. Maury, Eur. J. Inorg. Chem. (2009) 4357, and references therein.
[47] (a) F. Auzel, C. R. Acad. Sci. (Paris) 233 (1966) 819;
(b) F. Auzel, C. R. Acad. Sci. (Paris) 262 (1966) 1016.
[48] F.R. Gonçalves e Silva, O.L. Malta, C. Reinhard, H.U. Güdel, C. Piguet, J.E. Moser, J.-C.G. Bünzli, J. Phys. Chem. A 106 (2002) 1670.
[49] C. Reinhard, H.U. Güdel, Inorg. Chem. 41 (2002) 1048.
[50] M. Haase, H. Schäfer, Angew. Chem. Int. Ed. 50 (2011) 5808.
[51] M. Pollnau, D.R. Gamelin, S.R. Lüthi, H.U. Güdel, M.P. Hehlen, Phys. Rev. B61 (2000) 3337.
[52] F. Auzel, Chem. Rev. 104 (2004) 139.
[53] According to the long lifetime recently measured for Er($^4I_{13/2}$) in the molecular complex [CrErCr(**L3**)$_3$]$^{9+}$ (Table 2), the latter excited state is considered as the only energy storage reservoir.
[54] (a) D. Burdinski, F. Birkelbach, T. Weyermüller, U. Flörke, H.-J. Haupt, M. Lengen, A.X. Trautwein, E. Bill, K. Wieghardt, P. Chaudhuri, Inorg. Chem. 37 (1998) 1009;
(b) S. Ross, T. Weyhermüller, E. Bill, K. Wieghardt, P. Chaudhuri, Inorg. Chem. 40 (2001) 6656, and references therein.
[55] (a) O. Kahn, Adv. Inorg. Chem. 43 (1995) 179;
(b) R.E.P. Winpenny, Chem. Soc. Rev. 27 (1998) 447;
(c) O. Kahn, Acc. Chem. Res. 33 (2000) 647;
(d) C. Benelli, D. Gatteschi, Chem. Rev. 102 (2002) 2369;
(e) M. Andruh, J.-P. Costes, C. Diaz, S. Gao, Inorg. Chem. 48 (2009) 3342.